Miner Deposita
DOI 10.1007/s00126-007-0167-x

ARTICLE

The carbonate rock-hosted epithermal gold deposit of Agdarreh, Takab geothermal field, NW Iran—hydrothermal alteration and mineralisation

Farahnaz Daliran

Received: 7 April 2007 / Accepted: 2 October 2007

Abstract The disseminated gold deposit of Agdarreh (24.5 t at 3.7 g/t Au) is hosted in hydrothermally leached Miocene reefal limestone in the Takab geothermal field, which is part of the Cenozoic Urumieh–Dokhtar volcanic arc of NW Iran. Alteration and mineralisation are largely bedding controlled blanket-like and include: (1) pre-ore decalcification; (2) first-stage silicification associated with pyrite (early pyrite with 3–4 wt% As, late pyrite with <1–3 wt% As) and sphalerite; (3) second-stage silicification with precipitation of galena, Pb–Sb–As sulphides, sulphosalts, tellurides and native bismuth; (4) late-stage cinnabar and barite in vugs; (5) oxide ore stage and carbonate alteration (complex Mn–Fe-rich oxyhydroxides, arsenates, sulphates, APS minerals and rutile in residual leached rock and infill of karstic cavities). Gold occurs invisibly in the jasperoids and is enriched in the Mn–Fe oxyhydroxide surface cap of the jasperoids. Gold mineralisation is associated with the hydrothermal metal suite of As, Sb, Hg, Te, Se, Tl, Ba, Zn, Ag, Cd, Bi and Pb, and is characterised by very low Cu contents. Arsenian pyrite probably carried most of the primary (invisible) gold. Native gold occurs in association with the late-stage cinnabar and the oxide ore.

Editorial handling: B. Lehmann

The present paper deals with the geological framework, host rocks, characteristic features of hydrothermal alteration and mineralisation, and genesis of the Agdarreh deposit. The results of fluid inclusion and stable isotope studies are in progress and will be given in a forthcoming paper.

F. Daliran (✉)
Institute of Mineralogy and Geochemistry,
University of Karlsruhe,
Kaiserstr. 12,
76128 Karlsruhe, Germany
e-mail: farahnaz.daliran@img.uni-karlsruhe.de

The Agdarreh deposit shows many similarities with Carlin-type ore and is interpreted to have resulted from near-surface hydrothermal activity related to the Cenozoic arc volcanism that developed within the extensional Takab graben. The extensive oxidation at Agdarreh may be partly due to the waning stages of hydrothermal activity. Active H_2S-bearing thermal springs are locally depositing extremely high contents of Au and Ag, and travertine is present over large areas, suggesting that ore-forming hydrothermal activity occurred periodically from the Miocene to Recent in the Takab geothermal field.

Keywords Agdarreh · Gold · Carbonate rock-hosted · Epithermal · Takab geothermal field · Iran

Introduction

The Agdarreh mine (47°01′E 36°40′N) is one of two known gold deposits within the Cenozoic–Recent hydrothermal system of the Takab region in northwestern Iran. This region hosts an active geothermal field where thermal springs locally precipitate exceptionally high amounts of gold and silver, up to the kg/t level (Daliran 2003). There has been alluvial gold mining since antiquity in the area north of Takab, but the primary source of the gold was not known. The Agdarreh deposit was discovered in the late 1980s together with the neighbouring Zarshouran gold deposit and a number of gold prospects in the Cenozoic volcanic rocks of the region. Agdarreh is being mined by the Zarcan Company and contains a confirmed resource of 24.5 t Au with a potential gold resource of 30–60 t at a grade of 3.9 g/t gold (http://www.zarcan.com 2003, 2003).

The Agdarreh and Zarshouran gold deposits are hosted by carbonate-rich sedimentary rocks of Miocene and Upper Proterozoic–Lower Cambrian age, respectively, but they have several features in common and may belong to the same mineralisation system. They have been compared to Carlin-type deposits (Karimi 1993; Mehrabi et al. 1999; Asadi et al. 2000; Daliran et al. 2002) and may be referred to as sedimentary rock-hosted disseminated gold (SRHDG) deposits (Hofstra 2002).

Methods

Detailed geological and soil geochemical maps (Mineral Export Company 1995, 1996) were used as the basis for sampling of alteration and mineralisation at Agdarreh, whilst 1:100,000 maps of the Takht-e-Soleyman, Takab and Shahindezh areas (GSI 1999a, b, 2000) provided regional geological relations. Additional studies were carried out on the Zarshouran deposit and a number of active geothermal areas for regional comparisons.

More than 100 polished thin sections were prepared for petrographic and electron microprobe examination at the University of Karlsruhe. Electron microprobe analyses (EMPA) and X-ray images were used to locate and identify the very fine-grained sulphide and sulphosalt minerals, and the complex oxyhydroxides, silicates and carbonate minerals. Alteration minerals were identified by X-ray diffraction using a Siemens D5000 machine.

Pyrite is the main ore mineral at Agdarreh and could account for a significant proportion of the primary gold in the sulphide ore. Arsenic contents were systematically measured because the concentration of gold in pyrite is largely controlled by arsenic (Cook and Chryssoulis 1990; Simon et al. 1999; Cline 2001). Analytical data were obtained using a Cameca SX-50 electron microprobe and a REM Leo Gemini S4-10 scanning electron microscope. Sulphides and sulphosalts were analysed at 20 kV and 20 nA with a counting time of 30 s. Because of the complex composition of the oxide minerals and the lack of OH and H_2O data in electron microprobe analyses, the compositions of the hydroxide minerals are semi-quantitative. A few samples were tested for possible invisible gold at the Geological Survey of Finland using a Cameca SX-50 electron microprobe at 35 kV and 300–500 nA using the optimised CSIRO TRACE program (Robinson and Graham 1992), which provides a detection limit for gold of about 50 ppm.

Whole rock samples were analysed for trace elements by Actlabs (Ancaster, Canada) using inductively coupled plasma-optical emission spectroscopy (ICP-OES) after aqua regia extraction (Ag, Cd, Cs, Cu, Fe, Hf, Mn, Mo, Ni, Pb, Zn, Al, Ca, K, S, Ga, Ge, Se, Te, Tl, Bi), instrumental neutron activation analysis (INAA; Au, As, Sb, Ba, W) and the cold vapor fluid injection technique (FIMS-Hg).

Regional setting and metallogeny

The area hosting the Agdarreh and Zarshouran gold deposits is situated in northwestern Iran within the Urumieh–Dokhtar volcanic belt (Fig. 1). This belt formed as a result of the northward subduction of the Neo-Tethys along the Zagros thrust (Stöcklin 1968; Alavi 1994). The principal structure on a regional scale is the NNW-trending Geynardjeh thrust (a subsidiary of the Zagros thrust), along which the Angouran block has been thrust westwards onto the Takab basin (also called the Shirmard basin) (Fig. 2). Syn-extensional intra-arc faulting along reactivated crustal structures created a graben basin in the subsiding Takab block in Oligo-Miocene time (GSI 1999b). This tectono-morphological architecture causes a difference of elevation of more than 1,000 m between the overriding Angouran block and the subsiding Takab basin. Denuded, metamorphic basement rocks are exposed throughout the uplifted Angouran block, whereas the graben basin of Takab is filled by continental to shallow marine sediments of Oligo-Miocene to Recent age (Fig. 2). Sedimentation was accompanied by syn-extensional high-level magmatism (GSI 1999b; Stockli et al. 2004), volcanic activity and hydrothermal mineralisation. As in the Angouran block, the Takab basin is underlain by basement rocks that comprise metamorphosed pelite, psammite, carbonate and mafic volcanic rocks of Upper Proterozoic to Lower Cambrian age, and unmetamorphosed Cambrian to Ordovician formations.

In the Takab basin, the Lower Red Formation directly overlies the basement rocks and is part of an extensive Oligocene unit in Iran that comprises a transgressive continental red bed sequence of basal conglomerate, sandstone and marl, and evaporitic sediments (Alavi et al. 1982). The Lower Red Formation grades upwards into the Qom Formation comprising fine-grained detrital sediments with marl, tuff and limestone that is locally reefal. The gold deposit at Agdarreh is hosted by these reefal limestones (Aquitanian–Burdigalian) and is underlain by marly beds of Lower Miocene age. The Upper Red Formation overlies the Qom Formation and comprises red marl and sandstone with gypsum beds. Plio-Pleistocene coarse-grained clastic strata (3–4 Ma; Stockli et al. 2004) were deposited at the foot of the Geynardjeh thrust fault on the western margin of the Takab basin, suggesting that thrusting might still be active. Cenozoic sediments of the Takab basin are partially covered by Quaternary and Recent travertine, maar structures, dissected terraces of Quaternary fluvial sediments and Recent alluvium. Sediments of the Takab basin were gently

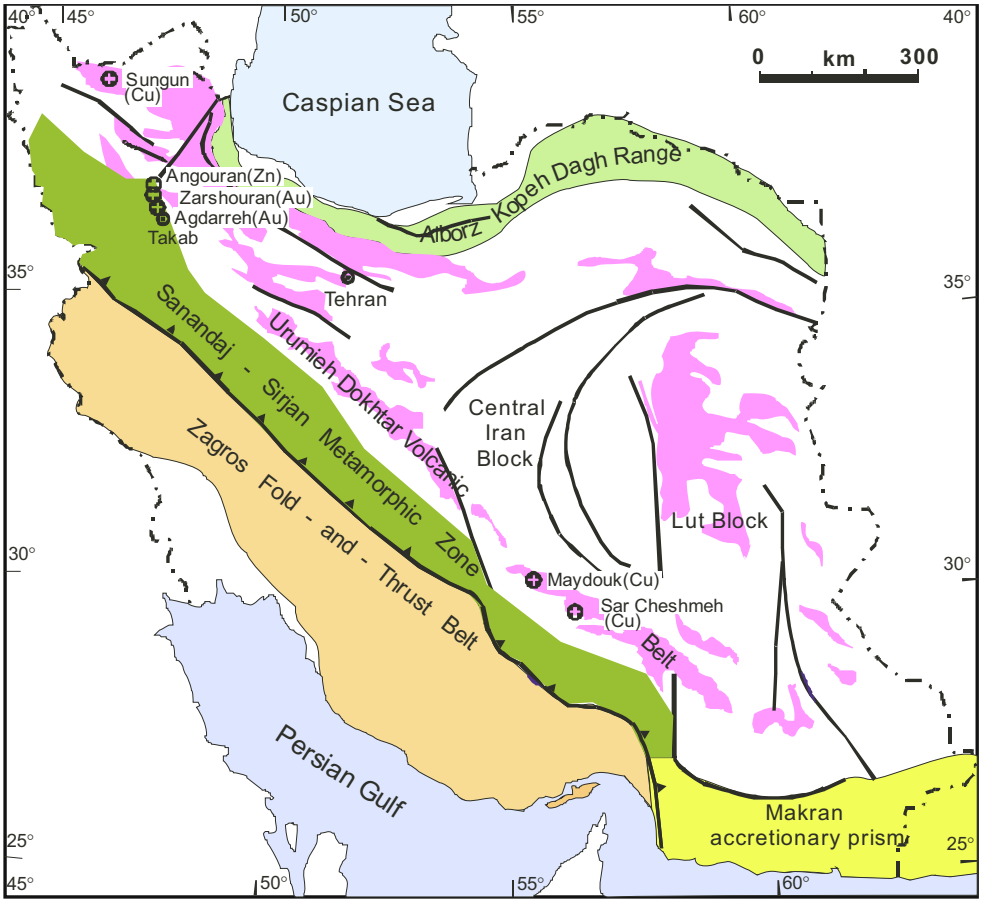

Fig. 1 Location of the Takab zone and the hydrothermal deposits of Agdarreh (gold), Zarshouran (gold) and Angouran (mixed sulphide–nonsulphide zinc) at the intersection of the Cenozoic–Quaternary volcanic belt of Urumieh–Dokhtar, which runs parallel to the Zagros thrust with the Sanandaj–Sirjan metamorphic zone. (Map courtesy of JL Lescuyer, modified from Stöcklin 1968)

folded during Alpine compression, which formed NW-trending fold axes sub-parallel to the Geynardjeh thrust fault.

Field relationships suggest that a white quartz porphyry was emplaced in the Lower Oligocene (pre-mineralisation) at Shakh-Shakh mountain directly north of the Agdarreh deposit, followed by Lower to Middle Miocene felsic to intermediate pyroclastic rocks, and Upper Miocene to Pliocene andesitic lava domes and sub-volcanic bodies (Ghorbani 2000). The andesites cover large areas and are spatially associated with gold mineralisation north of the Agdarreh and Zarshouran deposits. The andesites have been K–Ar dated at 16.2±0.3 to 14.4±0.3 Ma, and the overlying acidic volcanic rocks at 13.0±0.4 to 11.1±0.3 Ma, whilst the argillic alteration associated with the Zarshouran gold mineralisation is Ar–Ar dated at 14.2±0.4 Ma, demonstrating that mineralisation was contemporaneous with the Miocene volcanic activity (Mehrabi et al. 1999). A whitish, altered and weakly mineralised quartz porphyry in the area of the Zarshouran gold deposit is suggested to be of late Miocene to Pliocene age, based on regional correlation (Ghorbani 2000). Pliocene basalts occur south of the Takab region (Bidjar area) and have locally covered old riverbeds.

Several mineral occurrences are associated with Cenozoic volcanic–hydrothermal activity (Fig. 2). These include deposits of As–Au (Arabshah), Sb (Agdarreh Bala, Balderghani, Bakhirbulaghi), Hg (Shirmard, Yaraziz, Shakh-Shakh Mountain), Mn (Dabal Kuh), Fe (Shahrak, Kuh Baba), Pb–Zn (Aygalasi, Arpachay) and Zn(Au–Fe) (Chichaklou). On a regional scale, areas of extensive hydrothermal alteration with anomalous gold occur in andesites that show argillic alteration±alunite (Kalaki Mountain, Ayoubansar, Arabshah, Touzlar), and in sediments of the Qom Formation. The hydrothermal alteration has caused large-scale “sanding” of the basement carbonate rocks and also produced free carbon. Locally, gold mineralisation occurs in “sanded’ carbonate rocks that have also experienced silicification, e.g. the Zarshouran deposit.

Fault-hosted, vein and disseminated sediment-hosted deposits of gold, arsenic and antimony in the Takab region coincide with numerous dissected outcrops of travertine up to 100 km^2 in area and with thermal springs. The locations of the thermal springs are commonly controlled by faults, e.g. the intersection of NE-, NW- and E-trending faults at Takht-e- (or Zendan-e-) Soleyman. Solfataras of native sulphur and gypsum are closely related spatially to the sites of travertine deposits (e.g. at Gougerdchi), and liquid mercury has been reported by local villagers from some wells located within the red clastic beds. Thermal

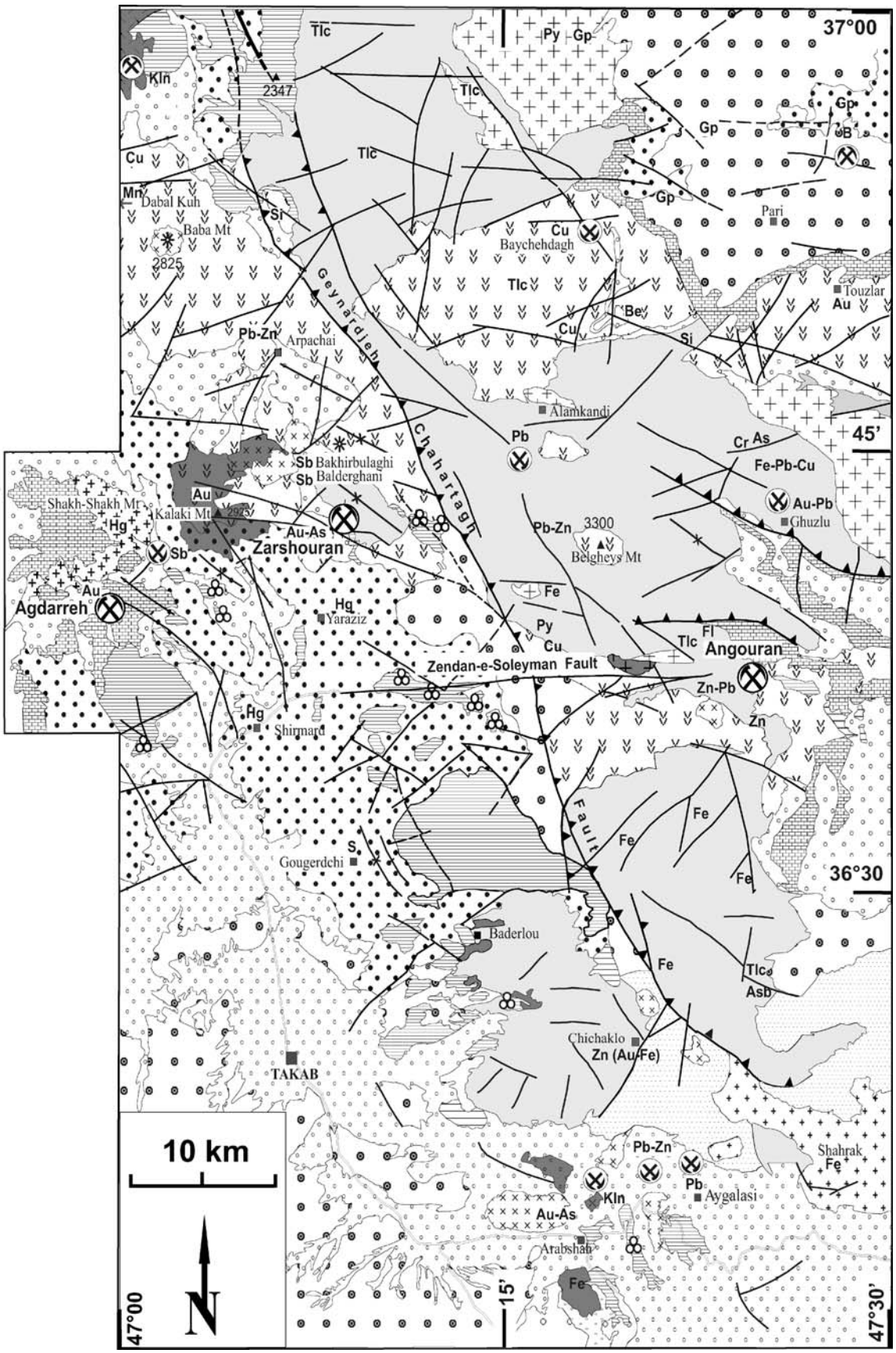
37°00
45'
36°30
47°00
15'
47°30'
10 km
N
Tlc
Py
Gp
Kln
2347
Cu
Mn
Dabal Kuh
Baba Mt
2825
Si
Baychehdagh
Pari
B
Touzlar
Au
Be
Pb-Zn
Arpachai
Geynardjeh
Chahartagh
Alamkandi
Pb
Cr
As
Fe-Pb-Cu
Au-Pb
Ghuzlu
Sb
Bakhirbulaghi
Balderghani
Shakh-Shakh Mt
Kalaki Mt
Hg
Au-As
Zarshouran
Pb-Zn
3300
Belgheys Mt
Agdarreh
Fe
Yaraziz
Py
Cu
Fl
Angouran
Zendan-e-Soleyman Fault
Zn-Pb
Zn
Shirmard
Fault
Gougerdchi
Baderlou
Asb
Chichaklo
Zn (Au-Fe)
TAKAB
Shahrak
Aygalasi
Arabshah

Fig. 2 (continued)

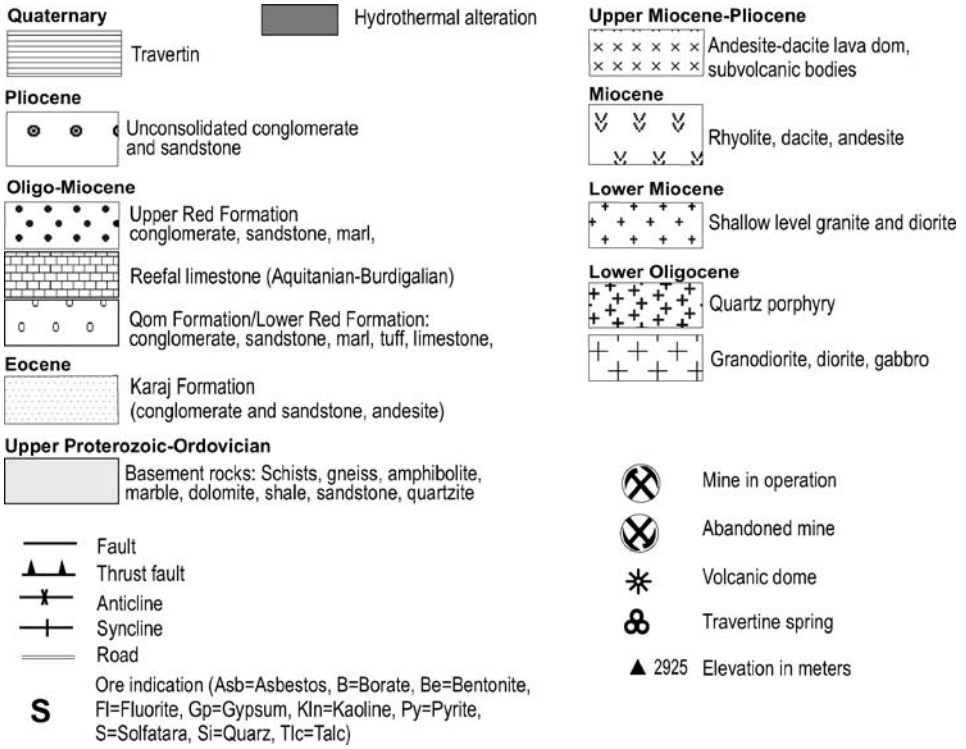

Fig. 2 Geology of the Takab geothermal field with the location of gold and other mineral deposits associated with Cenozoic to Recent volcanic–hydrothermal activity (modified after the geological maps of Takab, Takht-e-Soleyman and Shahindezh; GSI 1999a, b, 2000). Igneous rock ages are based on field relationships (Ghorbani 2002, personal communication)

springs continue to precipitate travertine and chemical mud that locally contain Cu, Se, Sb, Pb and As in the percent range, up to several thousand ppm Hg and Te, and up to 1,000 ppm Au and Ag (Daliran 2003). These various observations suggest that hydrothermal activity has continued from Miocene to Recent.

Geology of the Agdarreh deposit area

Massive cream-coloured reefal limestone of the Qom Formation (Aquitanian–Burdigalian) forms a 2,500-m high plateau that is the site of the Agdarreh gold deposit. This formation, which comprises biosparite to microsparite and micrite, and contains tabulate corals, is up to 150 m thick and occupies an area of almost 100 km^2. Weak karstic topography and a thin cover of terra rossa soil characterise the surface of the limestone. At Agdarreh, the reefal limestone overlies detrital and marly sequences of the Qom Formation, and is disconformably overlain by conglomerate and sandstone of the Upper Red Formation. White to cream sandstones and grits with rounded quartz pebbles in a kaolinite–illite-rich matrix occur in branching erosional channels developed upon the limestone, which suggests that uplift occurred with a change in the depositional environment from shallow marine to terrestrial. Travertine precipitates form small mounds of 40–50 m diameter on the flanks of the Agdarreh high (Fig. 3), and form a large field covering an area of 20 km^2 directly to the south of the Agdarreh deposit.

Structural data for the limestones in the Agdarreh area suggest that a gently folded dome is present. A series of subparallel normal faults and fractures cut the limestone, the most prominent of which are vertical to steeply inclined with a NNE to NW strike. Karst features, zones of weak hydrothermal alteration and brecciation, increased gold grades and soil geochemical anomalies all have a NE or NW orientation (Mineral Export Company 1996), thereby suggesting a structural control to the mineralisation. Although the faults are normal, some N- and NE-striking faults have a late strike–slip component as shown by subhorizontal slickensiding. Duplexes of strike–slip faults with the opposite sense of movement have formed dilatant zones that are locally silicified, brecciated and contain barite veins.

Outcrops with cauliflower-like erosional surfaces in a number of places have been previously mapped as tuffaceous rocks (Mineral Export Company 1995). These

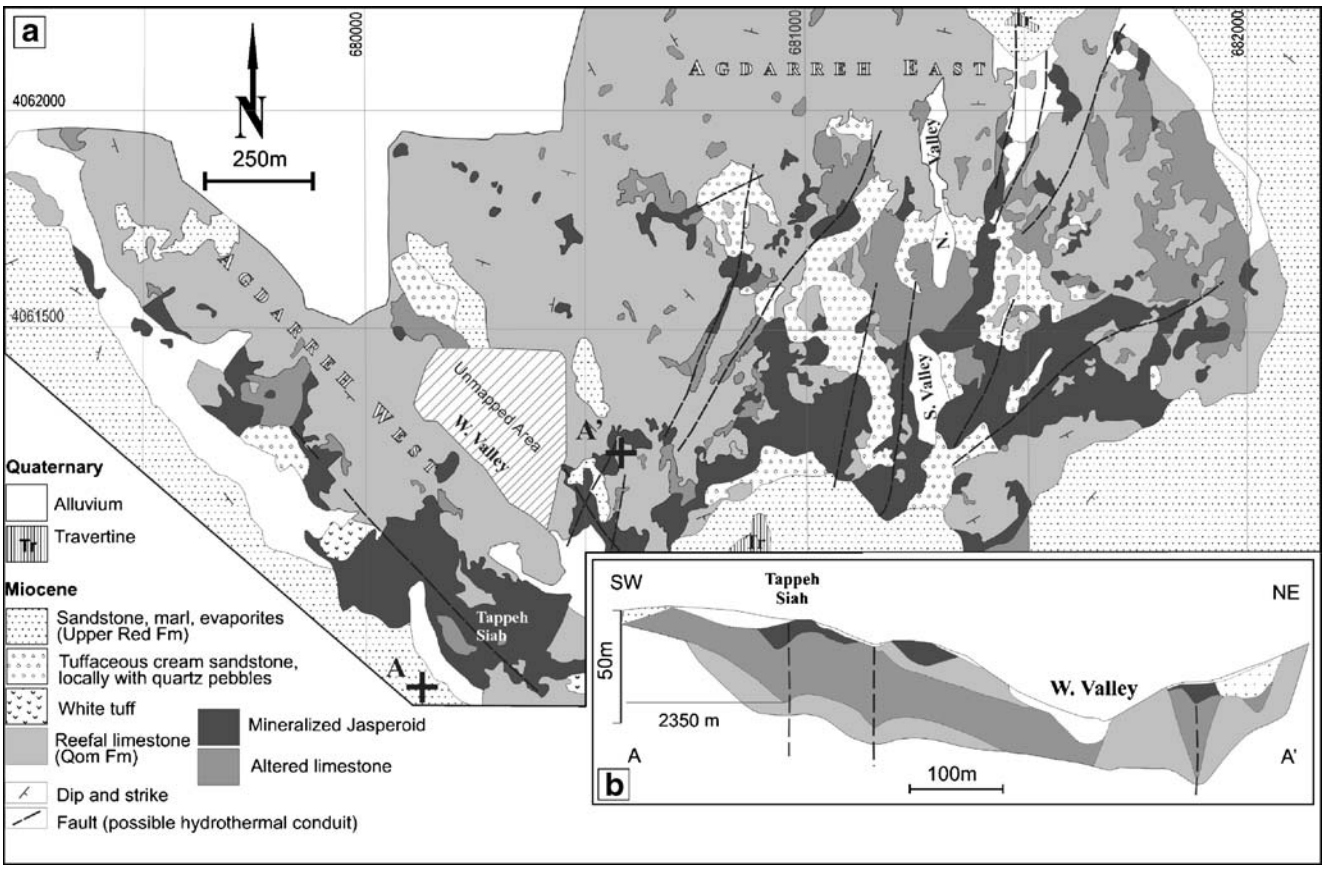

Fig. 3 **a** Geological map of the Agdarreh deposit showing the alteration and mineralisation zones of the host reefal limestone. **b** Drill profile showing the blanket-like geometry of the altered and mineralised zones, and the mineralised jasperoid cap (modified after Mineral Export Company 1995)

rocks, which have transitional contacts with normal limestones, consist mainly of quartz with reticulate microcrystalline texture and calcite with minor kaolinite and illite. They probably represent leached impure limestones rather than tuffs. At Tappeh Siah hill (means "black hill" in Farsi) at Agdarreh West, a chalky-looking white outcrop a few metres square occurs on top of the limestone and consists of embayed quartz grains and lithic clasts in a kaolinite–opal matrix. Based on remnant textures, this rock is an altered tuff, although the provenance is unknown.

Hydrothermal alteration and mineralisation

Gold is associated with zones of hypogene silicification and is enriched in the Fe–Mn-rich oxide blanket on top of the host reefal limestones (Fig. 4). The mineralisation located to date occurs from the surface down to 30 m depth (Zarcan International 2001, http://www.zarcan.com). The hydrothermally altered and mineralised rocks occur in two zones—Agdarreh East and Agdarreh West—which are divided by a structurally controlled NW-trending valley. Zones of silicification at Agdarreh East form NNE-aligned outcrops parallel to the fault system, indicating that the faults served as pathways to the mineralising fluids. At Agdarreh West, the silicified zones occur close to the NW-trending contact between the host limestone and the non-mineralised Upper Red Formation. Silicified bodies are blanket-like as a result of replacement of sub-horizontal limestone beds (Fig. 4).

On the basis of macroscopic rock textures, petrographic observations, XRD identifications and EMPA results, multiple hydrothermal events have been identified at Agdarreh. Extensive acid leaching of the host limestone was followed by pervasive silicification associated with a first stage of sulphide mineralisation. Second-stage mineralisation and silicification were accompanied by deposition of further sulphide minerals. During late-stage mineralisation, arsenic sulphides were formed and cinnabar was deposited with large amounts of barite. Widespread oxidation at Agdarreh then caused renewed acid leaching

Fig. 4 Field photograph of a circular travertine mound (*centre*) formed upon sandstones of the Upper Red Formation on the eastern flank of the Agdarreh high (*foreground*). The *white* formation in the background consists of an alternation of clastic rocks, marl and tuff of the Oligo-Miocene Qom Formation

of the limestone, precipitation of complex oxyhydroxides and gold enrichment (Table 1).

Pre-ore stage

Carbonate alteration

The most widespread alteration is carbonate dissolution resulting from the reaction of acid hydrothermal solutions with the limestone; in places, silicification accompanied this process. In the absence of silicification, carbonate leaching has turned the limestone into a porous, bleached chalky rock with a pitted surface (Fig. 5a). It is this type of altered limestone that has been mapped in places as tuff (Mineral Export Company 1995). Locally, carbonate dissolution has led to "sanding" of the limestone, i.e. the formation of granular, bleached rocks that crumble easily. Carbonate dissolution can also be caused by supergene acid leaching, which forms small karst cavities. This type of carbonate dissolution can be distinguished from hydrothermal leaching by the absence of silicification and formation of jasperoids. However, it is sometimes difficult to distinguish supergene (oxide stage) carbonate alteration from barren peripheral hydrothermal alteration.

Carbonate alteration can result in the replacement of primary sedimentary limestone by newly formed calcite and dolomite, and the coarsening of sedimentary calcite. Hydrothermal calcite is translucent and nucleates on dirty-looking primary sedimentary calcite; in places, hydrothermal calcite replaces newly formed dolomite (Fig. 5b). Newly formed calcite seldom occurs in the silicified carbonates and jasperoids. Dolomitisation occurs in pockets a few cubic metres in volume, especially at Agdarreh West. Electron microprobe analyses of newly formed calcite show elevated Mg contents relative to primary sedimentary calcite, which contains traces of Al, Si, K, P and Mg. Minor free carbon has been reported from drill holes at depths of 105–135 m (Persian Resources 1995). This carbon is commonly associated with abundant pyrite, indicating that reducing conditions prevailed at deeper levels.

Argillic alteration

Argillic alteration is uncommon at Agdarreh because of the low content of alumino-silicate minerals in the reefal limestones. However, the altered tuff at Tappeh Siah has undergone strong argillic alteration and the primary feldspars have been largely destroyed. In the limestones and the tuffs, kaolinite is more abundant than illite. Paragenetic relationships suggest that kaolinisation was partly the result of supergene acid leaching. Supergene kaolinite occurs as microscopic flakes in altered limestones, and as detrital accumulations in micropores and karst holes.

Ore stage I

Silicification

Pervasive silicification of the host limestone is the most common type of hydrothermal alteration at Agdarreh and has resulted in the formation of massive jasperoidal masses. Jasperoids do not occur in the altered tuff at Tappeh Siah.

Most jasperoids are conformable to bedding and form a flat-lying cap on top of the limestone, although discordant, fault-controlled silicification is also present. Silicified limestones vary from slightly silicified, partly porous,

Table 1 Bulk rock analyses of Agdarreh samples

Sample description	Au	As	Sb	Ba	Ag	Cu	Zn	Pb	Cd	Hg	Fe	Mn	Tl	Te	Se	K	Ca
Analytical method	INAA				ICP-OES					FIMS	ICP-OES						
Unit of measure	ppb	ppm	ppm	ppm	ppm	ppm	ppm	ppm	ppm	ppm	wt%	ppm	ppm	ppm	ppm	wt%	wt%
J-breccia	894	354	64	5,100	1	8	16	33	bdl	4	0.2	32	1.3	4.1	bdl	0.02	0.14
Mineralised J-Ba	367	490	125	11,000	4	15	161	328	2	55	0.5	141	3.5	1.3	0.6	0.01	0.21
HgS-bearing silica mud	42,900	5,200	8,900	93,000	30	9	46	8,692	bdl	2,200	0.6	56	45.8	17.8	2.6	bdl	0.29
HgS-bearing silica mud[a]	44,900	6,520	10,100	110,000	30	10	43	8,766	bdl	2,300	0.7	52	60.0	11.0	3.9	bdl	0.31
J-breccia-Ox-ore	342	886	166	20,400	0	5	34	122	1	38	0.1	18	1.6	0.7	0.2	0.01	0.08
HgS-rich J	342	269	219	bdl	3	4	22	313	bdl	2,900	0.1	65	1.0	11.6	1.2	bdl	0.06
Mineralised J-Ba	56	415	127	14,900	3	15	103	223	1	3	0.8	99	3.9	3.6	0.3	0.01	0.13
Mineralised J-Ba-Ox-ore	310	12,600	8,460	19,000	34	89	3,947	21,770	85	54	1.7	84	158.0	4.1	3.5	bdl	0.25
J-Ba-Ox-ore	405	6,590	1,550	16,000	7	16	21,590	10,026	456	77	9.6	>10%	78.2	3.5	2.5	0.06	0.34
Mineralised J-Ba-Ox-ore	70	1,220	482	2,600	2	13	1,533	989	22	34	2.1	15,920	14.6	2.4	0.1	bdl	0.32
Mineralised J-Ba-Ox-ore	205	5,750	2,590	78,000	9	46	5,075	10,050	110	26	0.3	2,597	12.2	9.9	0.7	bdl	0.17
SS-rich Q2-Ox-ore	250	9,800	2,940	2,300	97	692	35,560	23,288	852	77	7.2	>10%	56.8	30.2	22.1	0.04	0.40
Mineralised J-Ox-ore	2,080	2,620	145	1,940	2	6	2,655	494	8	14	1.1	42,580	32.6	4.1	bdl	0.09	0.31
Mineralised J-Ox-ore	680	4,180	758	2,800	4	5	6,801	2,660	57	29	10.3	>10%	48.4	6.5	0.6	0.02	0.26
Mineralised J-breccia-Ox-ore	13,000	10,700	1,340	8,900	bdl	2	41,440	182	74	400	5.6	>10%	256.0	8.5	2.4	0.06	0.46
Altered Lst-Ox-ore	2,840	25,600	333	5,900	6	15	20,490	1,005	107	190	6.8	>10%	1.1	0.7	bdl	0.03	10.80
Altered Lst-Ox-ore	94	8,400	105	200	bdl	2	12,130	40	7	6	7.1	>10%	99.0	15.9	1.2	0.10	18.15
Massive Ox-ore	95	2,390	821	6,000	1	bdl	8,869	575	47	23	7.5	>10%	68.3	5.3	0.5	0.02	0.34
Massive Ox-ore	20	3,400	2,830	9,000	bdl		2,860	226	44	19	8.2	>10%	189.0	7.6	0.3	0.03	0.45
Massive Ox-ore	bdl	4,570	2,500	8,300	1	10	11,070	302	12	bdl	8.6	>10%	23.9	3.1	0.8	0.01	0.28
Massive Ox-ore	671	31,100	684	bdl	6	6	90,250	1,908	443	75	8.3	>10%	699.0	4.8	6.6	0.17	2.55
Massive Ox-ore-Ba	4,610	9,500	1,050	55,000	3	17	43,980	2,061	59	180	20.3	>10%	19.8	14.5	6.7	0.03	0.28
Massive Ox-ore-Ba	685	31,500	1,170	2,600	4	13	60,810	1,515	371	220	14.6	>10%	150.0	5.2	5.9	0.19	1.66
Maasive Ba-Goethite	3,780	14,000	238	360,000	13	55	11,720	1,870	88	310	20.9	456	51.7	23.6	4.7	bdl	0.33
Mansfieldite, black	503	280,000	545	bdl	bdl	53	1,790	115	4	38	1.2	769	14.2	23.6	0.5	bdl	0.67
Mansfieldite, pink	153	320,000	74	bdl	bdl	30	737	13	1	bdl	0.4	155	6.8	7.6	0.2	bdl	0.86
Mansfieldite, pink	bdl	299,000	973	bdl	bdl	63	817	65	bdl	19	0.3	977	21.0	9.4	0.3	0.01	0.43
Mansfieldite, turquoise	bdl	313,000	569	bdl	bdl	7	426	9	bdl	20	0.2	25	4.4	13.4	0.7	bdl	0.19
Massive scorodite	5,950	220,000	335	880	2	14	733	422	2	bdl	22.8	19	86.8	16.8	6.5	0.20	0.31
Silicified Lst	836	63	14	970	bdl	3	21	9	bdl	11	0.1	31	0.3	2.0	bdl	0.04	0.10
Silicified Lst	238	1,200	59	330	bdl	5	101	98	1	10	0.2	175	11.4	2.7	0.4	0.04	28.33
Altered Lst	155	790	88	1,100	bdl	3	87	24	1	8	0.6	550	3.9	3.1	bdl	bdl	37.23
Altered Lst, green	87	1,900	41	150	bdl	3	205	8	1	9	0.3	369	6.7	1.4	bdl	bdl	31.96
Altered Lst, green	52	5,620	25	150	bdl	7	1,863	70	4	12	0.5	511	14.4	1.4	1.0	bdl	45.79
Altered Lst, green	342	12,900	568	1,800	bdl	9	437	1,418	13	14	1.3	1,687	2.9	8.2	0.4	0.01	44.27
Altered Lst, green	159	1,700	33	130	bdl	3	19	12	1	5	0.4	397	2.1	3.6	0.2	bdl	23.91
Altered Lst, red	131	1,830	279	6,110	bdl	17	3,271	98	8	11	6.5	5,730	14.5	3.3	1.0	0.01	36.39
Altered Lst, Ox-ore	506	483	8	240	bdl	5	113	18	bdl	12	0.1	1,575	3.0	bdl	0.7	bdl	43.78
Altered Lst-Ox-ore	46	850	27	bdl	bdl	bdl	514	33	2	4	1.5	63,096	0.5	1.9	4.8	0.03	38.87
Altered Lst-Ox-ore	28	210	10	3,400	bdl	2	bdl	9	bdl	3	0.1	19,963	0.9	1.4	0.3	bdl	41.95
Host Lst, unaltered	11	119	3	bdl	bdl	3	50	8	bdl	bdl	0.1	374	1.1	1.9	0.2	bdl	43.67
Host Lst, unaltered	5	158	2	bdl	bdl	3	25	20	bdl	bdl	0.1	1,616	0.3	bdl	0.7	bdl	47.23

All samples are from within the mineralised area of 1×0.75 km^2. Bi, Cs, Ga, Ge, Hf, Mo, Ni, and W were mostly below detection limit. Al and S have been omitted from the table because they were only partially recovered by the digestion method used.
Ba: barite, *J*: jasperoid, *Lst*: limestone, *Ox*: complex oxides, *Q*: quartz (stages 1 and 2), *S*: sulphides, *SS*: sulphosalts, *bdl*: below detection limit
[a] Duplicate sample.

leucocratic limestones to dark compact grey, commonly "vuggy" jasperoids. Textural and paragenetic relationships show that there have been at least two main stages of silicification, both with characteristic-associated sulphide minerals. In the mineralised zones, elevated levels of gold are associated with silicification (Zarcan International 2001, http://www.zarcan.com), but there are also barren jasperoids that lack gold and sulphides.

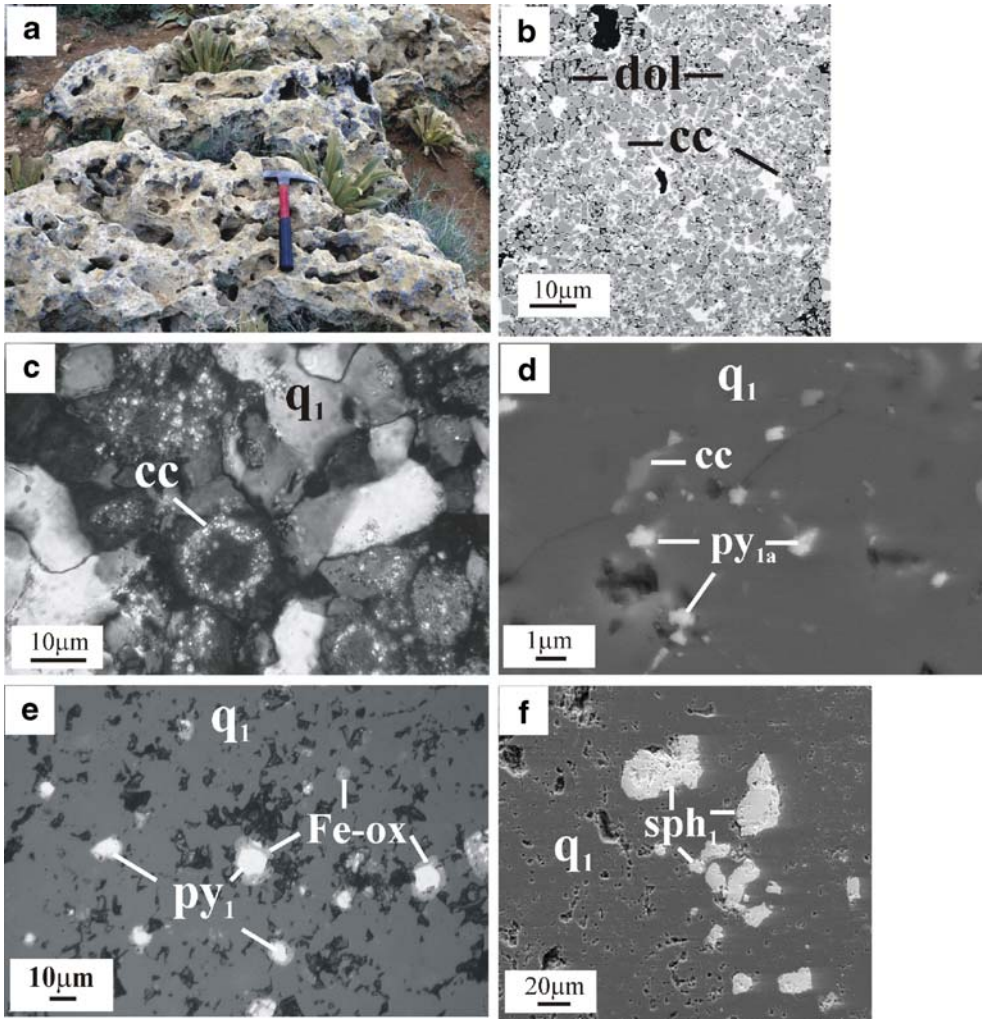

Fig. 5 Features of hydrothermal alteration and mineralisation of the pre-ore stage and the first ore stage. **a** Pitted weathering surface of the altered host limestone in a peripheral non-mineralised zone caused by the mechanical removal of the softer patches of leached and "sanded" limestone. **b** Sanded and dolomitised (*dol*) host limestone at Agdarreh West displays a later, probably supergene calcitisation (*cc*) along the grain boundaries. Dissolution and replacement along the grain boundaries has led to volume reduction, creation of porosity (*black* pore holes on the image), liberation of carbonate grains, and "sanding" (*BSE*). **c** Early stage quartz grains (q_1) display randomly arranged inclusions of Mn-bearing calcite (*cc*) that has precipitated along growth zones (*TCPL*). **d** Sub-micron inclusions of the earliest As-pyrite (py_{1a}) associated with Mn-bearing calcite (*cc*) enclosed in the early stage quartz (q_1; *BSE*). **e** First-stage pyrite (py_{1b}) is intergrown with first-stage quartz (q_1) in jasperoid. Pyrite grains are commonly oxidised to Fe oxyhydroxides (*Fe-ox*; *BSE*). **f** Agglomerations of first-stage sphalerite (sph_1) associated with first-stage quartz (q_1) in jasperoid (*BSE*). *TCPL* transmitted crossed-polarised light, *BSE* back-scattered electron image

Jasperoids display a variety of textures and grain sizes. In places, they exhibit a brecciated texture wherein relics of unaltered or less altered limestone are preserved, suggesting that volume loss and solution collapse occurred during alteration. First-stage quartz in jasperoids is commonly fine-grained, exhibits reticulate, xenomorphic and checkerboard-like textures and contains abundant carbonate inclusions that are occasionally randomly arranged along growth zones, indicating that the inclusions were newly formed (Fig. 5c). EMP analyses of the carbonate inclusions in quartz shows that, in contrast to the host limestone, they contain some Mn. The Mn in these inclusions was probably provided by early hydrothermal solutions and the carbonate by dissolution of the host limestone.

Rare, porous, cryptocrystalline jasperoidal rocks exhibit contorted cinnabar seams that are reminiscent of soft sediment deformation and were probably derived from silica mud. These rocks contain abundant, large (up to 1 cm), interlocked quartz crystals and barite. The quartz crystals contain common sulphide inclusions and are probably equivalent to the second-stage quartz.

Sulphide mineralisation

The sulphide mineralisation occurs disseminated and is associated with the two hydrothermal silicification stages. Although some sulphide minerals are common to both stages, each stage is characterised by a particular mineral assemblage. Most sulphides, including pyrite, have been oxidised and now only occur in minor to trace amounts. Sulphide minerals are very fine-grained and are almost invisible to the naked eye. Although galena and arsenic sulphides are rarely seen in polished section, the abundance of Pb oxide compounds and arsenates suggests that Pb- and As-sulphides were initially present in greater amounts. In contrast to galena, sphalerite is fairly abundant.

In the mineralised jasperoids, pyrite is the earliest and most abundant sulphide and can form up to 5–10% of the rock. The earliest pyrite generation (py_{1a}) typically occurs as sub-microscopic inclusions (<5 μm) in the first-stage quartz and is associated with newly formed carbonate inclusions (Fig. 5d). Most pyrite grains of this generation are smaller than the spots analysed by EMPA, and thus their initial metal contents have been "diluted" by quartz. However, a couple of reliable analyses show significant arsenic contents of 3–4 wt% (Table 2). Another pyrite generation (py_{1b}) is associated with the first-stage sphalerite, and both of these sulphides are interstitial to or intergrown with the first-stage quartz (Fig. 5e). Pyrite generation py_{1b} has lower arsenic contents ranging from <1 to 2.6 wt% As (Table 2) and has commonly undergone strong oxidation. Sphalerite is the second most abundant sulphide at Agdarreh (Fig. 5f). First-stage sphalerite has low contents of Fe (0.08 to 0.69 wt%), Cd (0.06 to 0.41 wt%) and Hg (0.00 to 0.80 wt%) (Table 3).

Ore stage II

Silicification

The first-stage quartz is crossed and brecciated by a second, coarse-grained quartz generation (Fig. 6a). Vugs in the jasperoids are commonly lined by the second-stage quartz

Table 2 Electron microprobe analyses of pyrite and arsenopyrite (wt%)

Host	Fe	S	As	Te	Sb	Cd	Ag	Zn	Cu	Pb	Tl	Hg	Se	Total
Early stage	43.73	50.80	4.42	na	na	na	na	na	na	na	na	na	na	98.95
	43.21	51.72	3.45	0.01	0.00	0.00	0.01	0.00	0.03	0.00	0.00	0.00	0.01	98.43
Ore stage I	44.28	52.28	2.63	0.03	0.07	0.00	0.01	0.09	0.00	0.00	0.00	0.03	0.00	99.42
	45.29	52.56	0.92	0.01	0.00	0.00	0.00	0.00	0.00	0.00	0.00	0.00	0.00	98.80
	44.34	53.49	0.64	0.04	0.03	0.00	0.00	0.04	0.06	0.00	0.00	0.08	0.00	98.72
	46.65	53.54	0.02	0.01	0.00	0.00	0.00	0.01	0.25	0.00	0.00	0.03	0.01	100.52
	43.81	51.86	2.89	na	na	na	na	na	na	na	na	na	na	98.56
	45.11	52.26	2.53	na	na	na	na	na	na	na	na	na	na	99.90
	45.25	52.25	1.59	na	na	na	na	na	na	na	na	na	na	99.09
	45.65	53.03	0.91	na	na	na	na	na	na	na	na	na	na	99.59
	45.18	52.79	0.37	na	na	na	na	na	na	na	na	na	na	98.34
Ore stage II	45.58	52.59	1.07	0.00	0.00	0.02	0.00	0.01	0.01	0.00	0.00	0.00	0.02	99.37
	44.66	52.83	0.52	na	na	na	na	na	na	na	na	na	na	98.01
	45.49	53.78	0.08	na	na	na	na	na	na	na	na	na	na	99.35
Inclusion in vug quartz (stage II)	43.49	54.17	0.03	na	na	na	na	na	na	na	na	na	na	97.69
	45.48	54.51	0.02	na	na	na	na	na	na	na	na	na	na	100.01
	46.05	53.95	0.00	na	na	na	na	na	na	na	na	na	na	100.00
Mn-bearing (Mn not quantified)	43.18	52.58	0.11	0.02	0.02	0.01	0.00	0.05	0.06	0.00	0.00	0.06	0.01	96.13
	43.34	53.20	0.25	0.01	0.01	0.01	0.01	0.03	0.00	0.00	0.00	0.04	0.00	96.93
"Silica mud"	42.19	47.07	8.48	0.01	0.30	0.00	0.00	0.00	0.01	0.21	0.00	0.22	0.04	98.55
	42.94	49.34	6.98	na	na	na	na	na	na	na	na	na	na	99.26
	42.83	49.38	6.23	na	na	na	na	na	na	na	na	na	na	98.44
	43.26	49.63	6.07	na	na	na	na	na	na	na	na	na	na	98.96
Arsenopyrite	36.16	29.34	35.06	0.03	0.36	0.02	0.03	0.02	0.02	0.33	0.00	0.05	0.14	101.57
	38.54	38.73	21.91	na	na	na	na	na	na	na	na	na	na	99.18
Silicified tuffs	44.89	52.08	2.09	na	na	na	na	na	na	na	na	na	na	99.06
	44.99	52.62	1.62	na	na	na	na	na	na	na	na	na	na	99.23
Oxide stage mansfieldite sinter	44.06	50.91	3.56	na	na	na	na	na	na	na	na	na	na	98.53

na: not analysed

Table 3 Electron microprobe analyses of sphalerite (wt%)

Host	Zn	S	Fe	Cd	Hg	Cu	Pb	Tl	Se	Te	Sb	Ag	As	Total
Ore stage I	63.44	33.51	0.69	0.36	0.11	bdl	bdl	bdl	0.01	bdl	0.03	bdl	0.03	98.20
	63.34	33.85	0.43	0.06	0.80	bdl	bdl	bdl	bdl	bdl	0.04	0.02	0.03	98.57
	65.50	33.12	0.38	0.22	0.07	0.01	bdl	bdl	0.02	bdl	bdl	bdl	bdl	99.32
	64.70	33.47	0.35	0.13	0.05	0.01	bdl	bdl	0.01	0.01	0.02	bdl	0.02	98.82
	65.39	33.10	0.28	0.38	bdl	0.03	bdl	bdl	0.01	bdl	0.01	bdl	bdl	99.18
	65.79	33.06	0.20	0.41	0.07	0.05	bdl	bdl	bdl	bdl	0.03	bdl	0.01	99.65
	65.39	33.56	0.19	0.22	0.05	0.03	bdl	bdl	bdl	bdl	0.01	0.03	bdl	99.51
	64.23	33.40	0.18	0.23	0.04	0.01	bdl	bdl	bdl	bdl	bdl	bdl	0.01	98.10
	64.08	33.47	0.17	0.35	0.05	bdl	bdl	bdl	bdl	bdl	bdl	bdl	0.03	98.15
	63.10	34.85	0.15	0.33	0.11	bdl	bdl	bdl	bdl	0.01	0.01	0.03	bdl	98.59
	64.62	33.24	0.13	0.28	0.04	bdl	bdl	bdl	bdl	bdl	bdl	bdl	bdl	98.31
	65.03	32.91	0.08	0.34	0.06	bdl	bdl	bdl	0.01	bdl	0.01	bdl	bdl	98.44
Ore stage II (inclusion in vug quartz)	61.43	33.17	2.09	0.42	bdl	bdl	bdl	bdl	bdl	bdl	0.03	0.02	bdl	97.19
	63.18	34.60	0.66	0.30	bdl	bdl	bdl	bdl	bdl	bdl	0.02	bdl	bdl	98.89
	63.12	33.27	0.40	0.38	bdl	0.02	bdl	bdl	bdl	0.01	0.02	bdl	bdl	97.23
	66.07	32.95	0.03	0.33	bdl	0.01	bdl	bdl	bdl	bdl	0.02	0.03	bdl	99.52
Rim	36.57	34.90	26.79	0.35	bdl	0.01	bdl	bdl	bdl	0.01	0.02	bdl	bdl	98.69
Core	39.21	34.80	24.33	0.33	bdl	bdl	bdl	bdl	0.03	bdl	0.02	bdl	bdl	98.79
Polhemusite	43.03	26.61	0.13	0.32	27.07	0.01	bdl	bdl	0.01	bdl	0.01	0.04	bdl	97.27

bdl: below detection limit

(Fig. 6b), which can form euhedral crystals up to 7 cm long that are locally arranged as rosettes. Quartz crystals commonly have a milky base with myriad fluid inclusions, but a transparent terminated end. The cores of second-stage quartz grains are optically homogeneous with multiple growth zones defined by minute fluid and carbonate inclusions. The margins of second-stage quartz grains display plumose, spherulitic or undulose extinction. Rare inclusions of Ba–Ca–strontianite occur within these quartz crystals, whereas sulphide minerals and acicular inclusions of Pb sulphosalts occur at the rims of the crystals.

Sulphide mineralisation

The second-stage quartz is associated with a second generation of pyrite (py_2) and sphalerite (sph_2). $Pyrite_2$ occurs as euhedral to sub-hedral crystals up to 30–40 μm; in places, exhibits a sieve texture and corrosion embayments. $Pyrite_2$ also occurs as inclusions with Pb sulphosalts in vug quartz and in sphalerite. Larger pyrite grains occasionally exhibit growth zoning (Fig. 6c) with first-stage As-enriched pyrite overgrown by second-stage relatively As-poor pyrite. Pyrite framboids with coarsened rims are locally abundant in pore spaces in the jasperoids (Fig. 6d). Rare colloidal aggregates of Mn-bearing pyrite may have resulted from late Mn-bearing solutions. Most of the py_2 grains contain <1 wt% As (Table 2). Pyrite inclusions in the second-stage quartz crystals in the "silica mud" contain 6–8 wt% As, the highest values recorded in pyrite from Agdarreh. Rare arsenopyrite was found as skeletal and rhombic crystals in the "silica mud", closely associated with As-rich pyrite (Fig. 6e) and rare As-sulphides (orpiment) (Table 2), suggesting that the ore fluids were enriched in arsenic.

$Sphalerite_2$ grains are large (up to 100 μm) and commonly contain different inclusions of pyrite, galena, Pb sulphosalts, altaite, native Bi, F–apatite and quartz (Fig. 6f). $Sphalerite_2$ shows higher Fe contents (0.03 to 2.09 wt%) than sph_1 and contains Cd (0.33–0.42 wt%) (Table 3). Large sphalerite inclusions (120 μm) in vug-filling quartz crystals are ferroan with 24.3 to 26.8 wt% Fe. Some overgrowths on $sphalerite_2$ consist of polhemusite ([Zn, Hg]S) containing 43.0 wt% Zn, 27.1 wt% Hg, 0.32 wt% Cd and 0.13 wt% Fe) (Table 3). $Sphalerite_2$ associated with Pb sulphosalts in vug-filling quartz rosettes contains only 0.66 wt% Fe with 0.33 wt% Cd (Table 3).

Lead minerals presently occur mainly as inclusions in second-stage quartz, but are also found in $sphalerite_2$ (Fig. 7a). Pb sulphosalts are closely associated with galena or occur as exsolutions in galena. Galena is less common and contains minor Sb (0.28 to 0.56 wt%) and traces of Ag (<300 ppm). Most Pb sulphosalt grains have the composition of twinnite ($Pb[Sb,As]_2S_4$). Twinnite contains 0.17 to 0.31 wt% Ag and 0.04 to 0.53 wt% Cu with traces of Zn, Fe and Se. Geocronite ($Pb_{14}[Sb,As]_6S_{23}$) occurs as exsolved lamellae in galena (Fig. 7b) and contains traces of Cd, Te, Se, Ag, Cu and Zn. Other Pb-bearing minerals include boulangerite ($Pb_5Sb_4S_{11}$) with traces of Ag and As, and semseyite ($Pb_9Sb_8S_{21}$) with traces of Cd, Ag, Cu, Se and As. Some worm-like inclusions in the vug-filling quartz have formulae close to $[Pb_{0.97}Tl_{0.03}][As_{1.47}Sb_{0.53}]_2{\cdot}S_{3.18}$ and

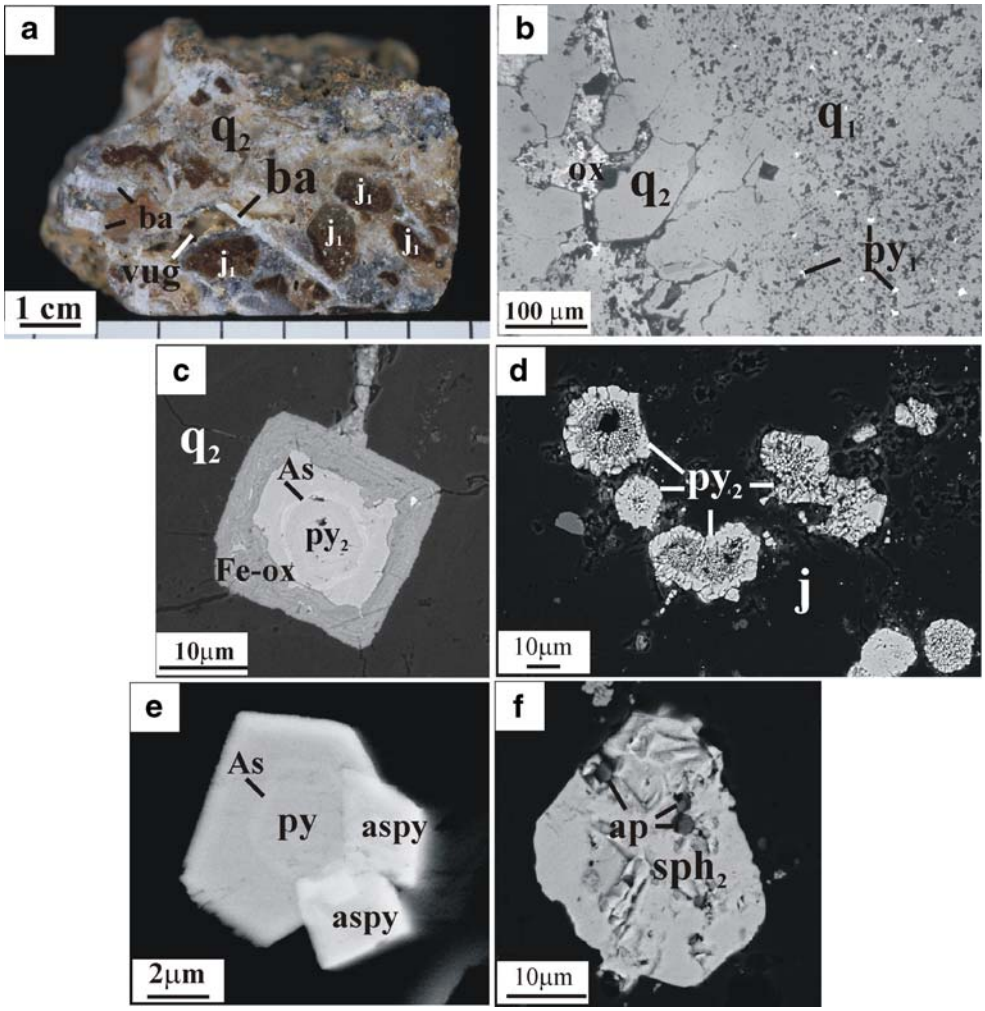

Fig. 6 Typical ore texture and minerals of the second ore stage. **a** Polished slab of matrix-supported hydrothermal breccia showing cross-cutting relationships between the first, second and late ore stage minerals. *Brownish* clasts consist of first-stage quartz-pyrite (j_1) in a matrix of second-stage quartz 2 (j_2). Both stages are cross-cut by late-stage platy barite (*ba*) that penetrates open spaces and vugs coated by j_2. **b** Photomicrograph showing first-stage fine-grained quartz (q_1) and pyrite (py_1) cross-cut by coarse-grained translucent second-stage quartz (q_2) growing onto the pore spaces. (*ox*) is an oxide-stage Mn–Fe oxyhydroxide filling (*TPPL*). **c** Growth zoning of second-stage pyrite (py_2) marked by discrete, As-rich (lighter) zones (*BSE*). Pyrite is oxidised to Fe oxyhydroxides along the grain boundary (Fe-ox). (q_2) is second-stage quartz. **d** Framboidal pyrite (py_2) with coarsened rim in the pore spaces of jasperoid (*j*; *BSE*). **e** Micron-size crystals of As-rich pyrite (*py*) intimately interlocked with arsenopyrite (*aspy*) in "silica mud". Note the discrete, arsenic-rich zone (lighter, As) in pyrite (*BSE*). **f** BSE image of second-stage sphalerite (sph_2) enclosing inclusions of F–apatite (*ap*; *BSE*). *TPPL* transmitted plane-polarised light, *BSE* back-scattered electron image

$[Pb_{0.94}Ag_{0.05}][As_{1.3}Sb_{0.75}]_{2.04}S_{3.95}$ (Table 4). These inclusions are similar to twinnite but have a higher As/Sb ratio and might represent a new Pb sulphosalt. Sphalerite$_2$ also contains sub-microscopic inclusions (approximately 1 µm) of altaite ($PbTe_2$).

Rare getchellite ($AsSbS_3$) occurring as inclusions in vug-filling quartz was also formed in the second sulphide stage (Fig. 7c). Rare native Bi occurs as sub-microscopic grains in minute vugs in the jasperoidal rocks (Fig. 7d), as inclusions in sphalerite$_2$ and barite, and in various altered carbonate rocks.

Although supergene arsenates such as scorodite and mansfieldite are common, arsenic sulphides are rarely encountered. Visible arsenic sulphides were found as late vug fillings in a few jasperoid samples. Sub-microscopic relics of orpiment (Table 4) are occasionally found in the jasperoidal "silica mud" and in Mn–Fe-rich oxyhydroxide rocks where they contain traces of Se.

The Cu content of the sulphide minerals is very low (ppm to tens of ppm), which is in accord with the lack of individual Cu minerals (see also Table 1). The highest Cu contents (0.4 to 0.5 wt%) are in the Pb sulphosalts. Although the jasperoids contain up to 256 ppm Tl, discrete Tl minerals have not as yet been identified, although a number of Tl minerals occur in the nearby Zarshouran gold deposit (Karimi 1993; Mehrabi et al. 1999; Asadi et al. 2000).

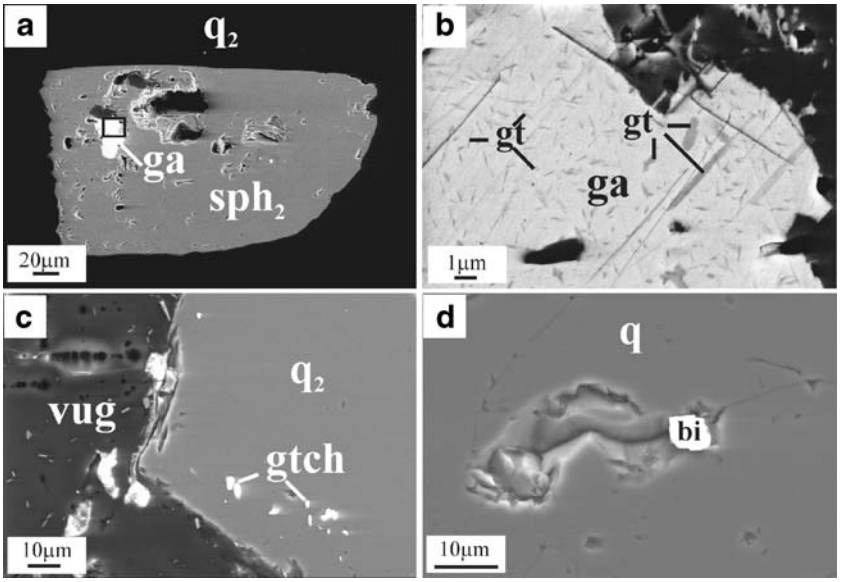

Fig. 7 Back-scattered electron images of second ore stage Pb sulphides and sulphosalts, and native bismuth. **a** Sphalerite grain (sph_2, Fe-rich) within a large late-stage quartz crystal (q_2) contains inclusions of Pb sulphides (*ga*) and Pb sulphosalts (invisible here). **b** Enlargement of boxed area in **a** showing exsolution lamellae of geocronite (*gt*) within galena (*ga*). **c** Getchellite inclusions (*gtch*) in the peripheral zone of a late quartz crystal (q_2). Bright grains bordering quartz grains in the vug are Pb–Fe arsenates. **d** Native Bi grain (*bi*) in tiny vug in silicified limestone (*q*)

Late ore stage: cinnabar and barite

Mercury sulphides were formed during the very late, post-silicification stage of hydrothermal activity, in vugs in the jasperoidal rocks, and are paragenetically associated with barite (Fig. 8a and b). Narrow seams, spots, spicular grains, skeletal growths and disseminations of cinnabar occur in the "silica mud" and are associated with abundant platy

Table 4 Electron microprobe analyses of Pb sulphides and sulphosalts, and As sulphides (wt%)

Host	Pb	S	Sb	As	Ag	Te	Cd	Zn	Cu	Fe	Tl	Hg	Se	Total
Inclusions in rosettes of vug quartz (ore stage II)														
Galena	86.15	13.60	0.56	0.01	0.13	bdl	0.07	bdl	bdl	bdl	bdl	bdl	0.01	100.54
	85.55	13.51	0.28	0.02	bdl	0.11	0.27	0.05	0.04	0.06	bdl	bdl	bdl	99.90
Geochronite	65.21	16.73	11.75	3.41	0.01	0.01	0.09	0.05	0.01	bdl	bdl	bdl	0.01	97.29
	64.94	16.75	11.72	3.32	0.07	bdl	0.04	bdl	0.04	0.04	bdl	bdl	0.02	96.94
Boulangerite	55.53	18.93	25.72	0.26	0.08	0.01	bdl	bdl	0.01	0.01	bdl	bdl	bdl	100.55
Semsyite	51.64	18.93	27.12	0.19	0.03	bdl	0.02	bdl	0.05	0.01	bdl	bdl	0.02	98.00
Twinnite	32.10	23.42	38.30	4.55	0.25	bdl	bdl	bdl	0.45	0.01	bdl	bdl	0.05	99.13
	32.94	23.71	37.92	4.89	0.29	bdl	bdl	bdl	0.37	0.01	bdl	bdl	0.03	100.17
	33.82	23.81	33.98	6.19	0.25	0.01	0.04	0.02	0.52	0.01	bdl	0.01	0.05	98.74
	32.44	23.78	35.16	7.81	0.31	bdl	0.01	0.05	0.43	0.02	bdl	bdl	0.05	100.06
	34.56	24.28	32.91	7.02	0.20	0.04	bdl	bdl	0.53	bdl	bdl	bdl	0.04	99.63
	33.36	22.50	34.84	6.79	0.24	bdl	bdl	0.02	0.42	0.01	bdl	bdl	0.05	98.25
	32.47	22.85	36.08	5.62	0.19	0.02	0.01	0.01	0.54	0.01	bdl	bdl	0.04	97.84
	32.12	22.50	37.28	5.28	0.27	bdl	bdl	0.03	0.5	0.02	bdl	0.02	0.01	98.05
	32.16	22.13	39.43	4.41	0.24	bdl	bdl	bdl	0.43	0.03	bdl	bdl	0.02	98.85
	32.50	24.19	41.97	1.92	0.17	bdl	bdl	0.01	0.04	0.01	bdl	bdl	0.01	100.87
New sulphosalt?	39.36	24.92	12.68	21.55	bdl	bdl	0.03	bdl	bdl	0.02	1.42	bdl	0.06	100.09
	37.44	24.34	17.68	18.58	1.05	bdl	0.04	0.04	bdl	0.05	0.16	bdl	0.06	99.44
"Silica mud"														
Galena	86.15	13.60	0.56	0.01	0.13	bdl	0.07	bdl	bdl	bdl	bdl	bdl	0.01	100.54
	85.55	13.51	0.28	0.02	bdl	0.11	0.27	0.05	0.04	0.06	bdl	bdl	bdl	99.90
Orpiment	bdl	37.40	0.03	61.40	0.01	bdl	bdl	0.04	0.01	0.10	bdl	bdl	0.29	99.30

bdl: below detection limit

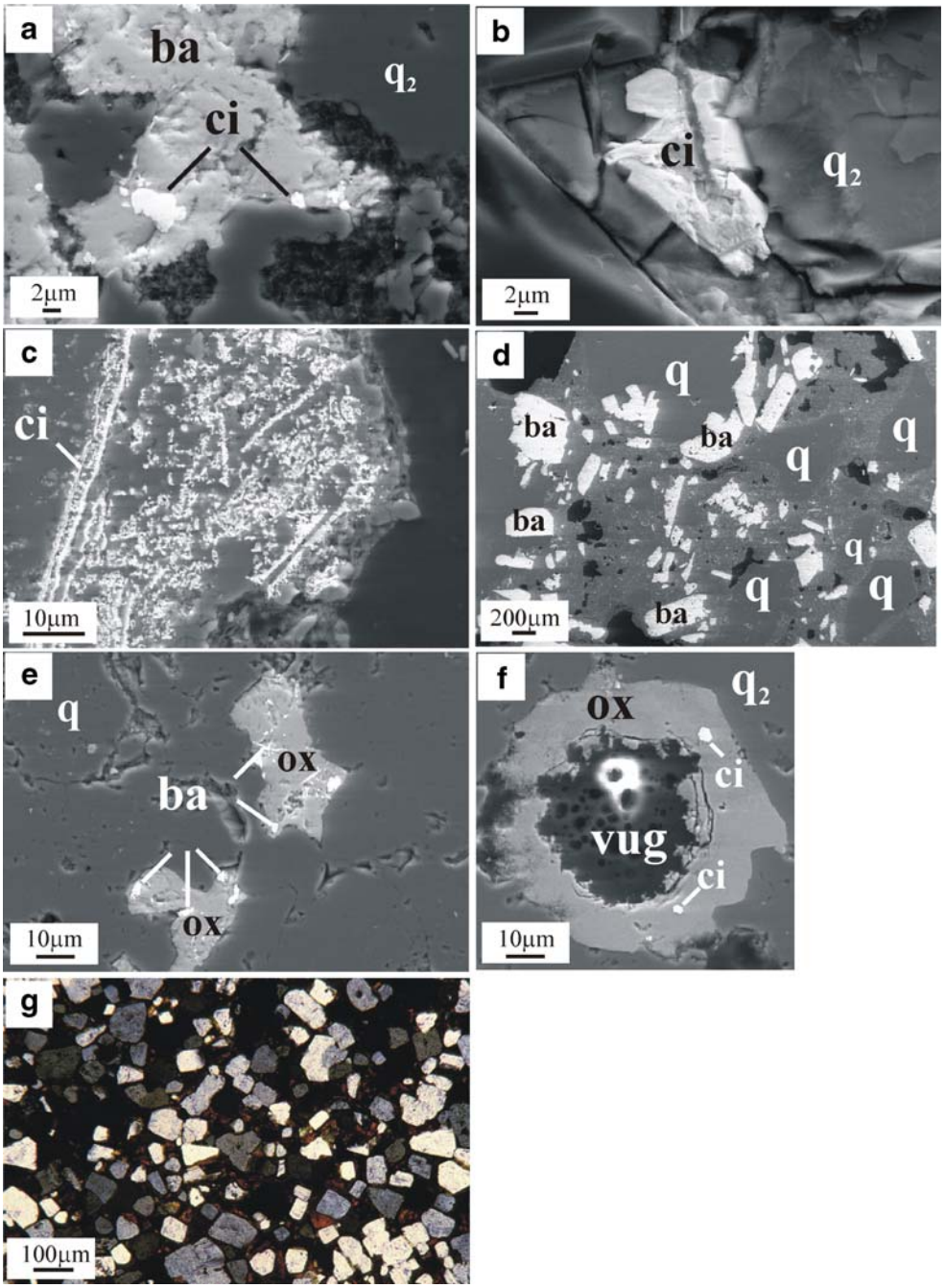

Fig. 8 a–f Back-scattered electron images of late ore stage Hg-sulphides and barite. **a** Paragenetic association of cinnabar (*ci*) and barite (*ba*) in vugs of second-stage quartz grains (q_2). **b** Cinnabar crystal (*ci*) in jasperoid void (q_2). **c** Fine seams of skeletal cinnabar (*ci*) in "silica mud". **d** "Silica mud" consisting of abundant crystals of bladed barite (*ba*) and quartz (*q*) in a cryptocrystalline matrix of quartz and cinnabar (salt and pepper appearance). **e** Barite (*ba*) associated with Fe–Mn oxyhydroxides (*ox*) in jasperoid vugs (*q*). Note needle-like (skeletal) habit of barite in this association. **f** Simultaneous precipitation of cinnabar (*ci*) and Fe–Mn oxyhydroxides (*ox*) coating a vug within late-stage quartz crystals (q_2). **g** Photomicrograph showing abundant barite crystals (*grey* to *white shades*) in oxide-stage (*goethite*) matrix (*black*; transmitted plane-polarised light)

barite and euhedral quartz crystals (Fig. 8c and d), which suggests that these rocks were formed during the latest hydrothermal activity and probably near the surface. Cinnabar seams are associated with pyrite (including a framboidal type), arsenopyrite, orpiment, kaolinite, rutile, zircon and La–Ce-bearing aluminium phosphate sulphate minerals (APS). Cinnabar commonly contains trace amounts of silver (0.05–0.13 wt%) and minor amounts of Fe (up to 1.7 wt%) (Table 5). Rare mercury sulphide grains contain Br and Cl, which suggests that corderoite ($Hg_3S_3[Cl,Br]_2$) is present.

Hydrothermal barite mainly occurs as isolated blades, reticulate masses, veins and networks in altered limestone, silicified limestone and jasperoids. Platy barite forms crystals up to 10 cm in length and rarely contains inclusions of sulphides and native bismuth.

The formation of barite and cinnabar has continued into the oxide stage. Vugs in jasperoids filled or lined by Mn–Fe oxyhydroxides contain occasional minute inclusions of skeletal barite and cinnabar (Fig. 8e and f). Massive goethite–barite rocks that are locally present in the oxide ore zone consist of authigenic barite crystals in a matrix of

Table 5 Electron microprobe analyses of Hg-sulphides (wt%)

Host	Hg	S	Fe	Sb	Cd	Ag	Zn	Cu	Pb	Tl	Te	Se	As	Total
Jasperoid	83.58	12.58	1.73	bdl	0.01	0.11	0.08	0.01	bdl	bdl	bdl	bdl	0.05	98.15
	87.43	12.77	0.25	0.04	0.02	0.05	0.85	bdl	bdl	bdl	0.06	bdl	0.10	101.57
"Silica mud"	87.19	12.61	0.01	bdl	bdl	0.08	0.01	bdl	bdl	bdl	0.04	0.03	0.02	99.98
	87.97	12.70	bdl	0.06	0.04	0.12	0.04	bdl	bdl	bdl	0.01	bdl	bdl	100.94
	88.80	12.62	0.01	bdl	bdl	0.13	bdl	bdl	bdl	bdl	bdl	bdl	bdl	101.59

bdl: below detection limit

goethite and are probably supergene (Fig 8g). Mercury sulphides are occasionally enclosed in the massive oxide ore, and are associated with native Bi, F–apatite and APS minerals.

Oxide stage

Extensive supergene acid alteration has largely decomposed the sulphide minerals and redeposited the metals within an irregular blanket of Mn–Fe-rich oxide ore throughout the Agdarreh deposit. The oxide blanket crops out as rubbly to powdery friable masses of crustiform to botryoidal, black, mixed Mn–Fe oxyhydroxide rocks and ochrous Fe-rich oxyhydroxides. The oxyhydroxide minerals also fill cavities in jasperoids and in places replace the host limestone. The oxide ore zone generally grades downward into barren altered limestones. Drill hole results show that the oxide blanket occurs at an average depth of 30–35 m and is enriched in gold (Zarcan International 2001, http://www.zarcan.com). A whole-rock analysis of oxide ore yielded 22.8 wt% Fe, >10% Mn, 9 wt% Zn and 2.3 wt% Pb (Table 1).

Oxide-stage acid leaching caused renewed carbonate dissolution of the limestone and some limestones were totally replaced by Mn–Fe oxyhydroxides (Fig. 9a). Dissolved carbonate was reprecipitated as microveins of white calcite within the oxide ore or as vug fillings in the oxide ore (Fig. 9b and c). In some instances, it is difficult to know whether carbonate alteration was related to peripheral hydrothermal activity or was generated by supergene processes. Where limestone is replaced by late calcite, rare carbonates of Ca–Mg–Mn, Pb–Fe–Mn, Fe–Mn, Fe and Mn–Zn are present.

Slight alteration of limestone is characterised by patinas and impregnations of scorodite, an increase in porosity and spotting caused by recrystallised calcite and/or Mn oxides and minor newly formed "authigenic" quartz (Fig. 9d). Scorodite is a common oxide-stage mineral that occurs with jarosite and occasionally forms massive rocks.

Altered limestone also contains aluminium–phosphate–sulphate (APS) minerals as pore-fillings (Fig. 9e) and as disseminations of sub-microscopic grains associated with F–apatite. The APS minerals are isomorphous with alunite and have the general formula $RAl_3(PO_4)_{1-x}(SO_4)_{1-x}(OH)_6(H_2O)_x$ with R–Pb, Fe, Sb, Zn, Mn, Ca, Cd, Si, La, Ce, Sr and Ba. The most common cations are Pb and Pb–Fe; $(AsO_4)^{3-}$ predominates over other anions and anionic radicals. Phosphates of the pyromorphite–mimetite series are also present and are locally Sb-bearing. Less common are Zn arsenates and Fe–Mn arsenates such as ferroan zincian mimetite (Fig. 9f) and Fe–Ca arsenate–phosphate minerals.

Metre-scale outcrops, which have the appearance of sinter (Fig. 9g), are laminated, porous, opaline-looking and white to pale coloured. This material was identified by XRD and EMPA as mansfieldite ($Al[AsO_4]\cdot 2H_2O$) with 32 wt% As (Table 1). The presence of mansfieldite-cemented regolith suggests that the sinter-like masses have been formed on the surface. Minor amounts of quartz, pyrite (Fig. 9h), strengite, melanterite, scorodite, kaolinite, alunite and gypsum are associated with mansfieldite. Irregular veins, balls and laminae of opaline silica and white gibbsite–bayerite ($Al(OH)_3$) have formed close to the mansfieldite rocks.

During the oxide stage, dispersed "authigenic" quartz crystals (<20–30 μm) were precipitated with the oxides. Oxide-stage quartz locally contains minute inclusions of manganoan calcite, Mn oxides, scorodite, F–apatite, La–Ce phosphates, and Ca-sulphate. Growth zones in oxide-stage quartz crystals are occasionally marked by Mn oxyhydroxides. Quartz in the mansfieldite rocks contains inclusions of framboidal pyrite and rare droplet-shaped cinnabar.

Gold distribution

All rocks anomalous in gold contain sulphide minerals or Mn–Fe oxyhydroxides (Table 1; Persian Resources 1995; Zarcan International 2001, http://www.zarcan.com). This suggests that gold was initially associated with sulphide minerals and was later re-mobilised into the Fe–Mn oxyhydroxides. It is possible that much of the

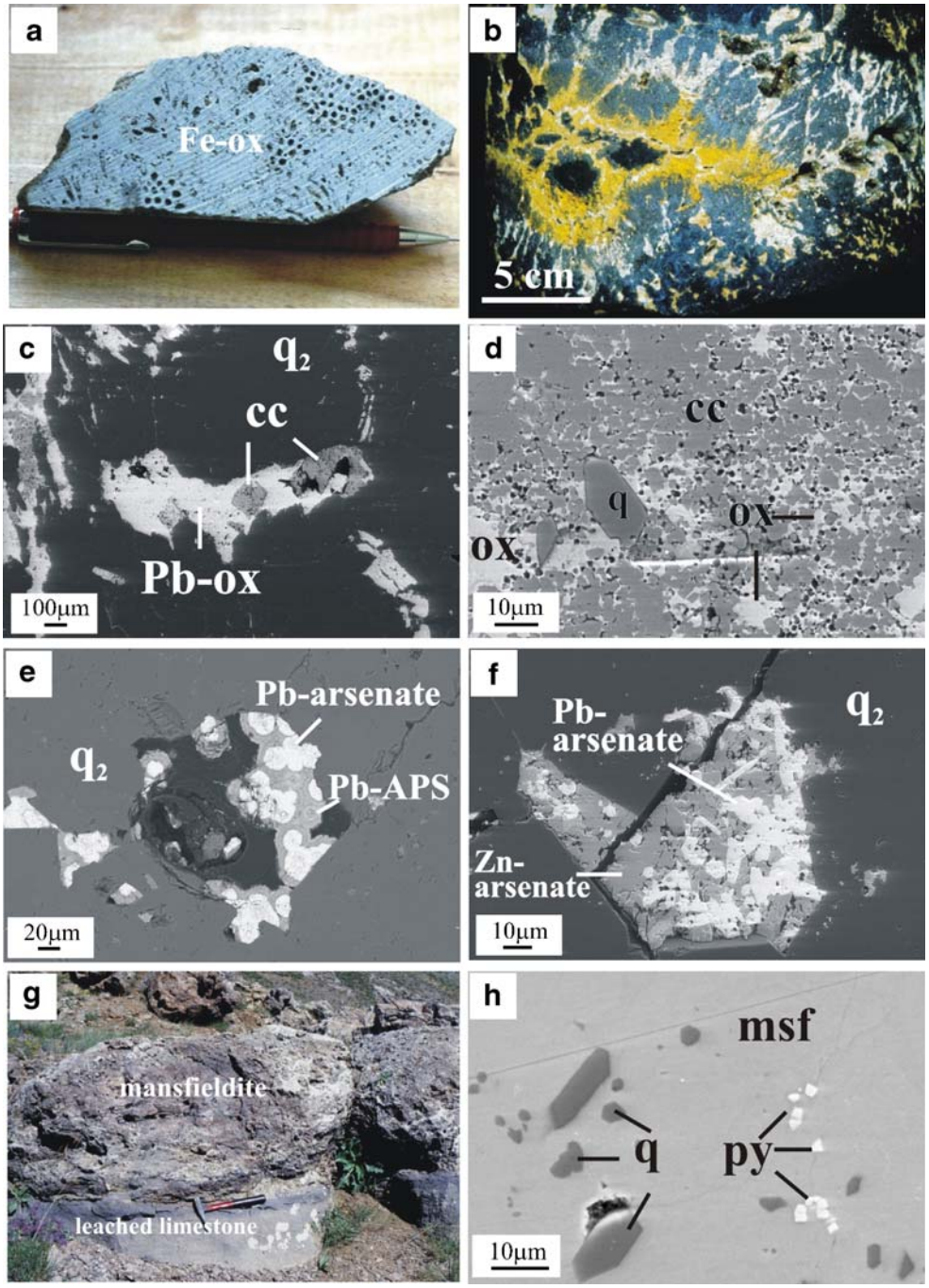

Fig. 9 Oxide-stage alteration and ore minerals. **a** Polished slab of a black oxide ore sample showing replacement of corals of the reefal limestone by Fe–Mn oxyhydroxides (*Fe-ox*). **b** Oxide stage carbonatisation represented by *white* calcite veins cutting through the *black* oxide ore. The *yellowish* crust is jarosite. **c** Euhedral oxide-stage calcite (*cc*) and Pb oxide complexes (*Pb-ox*) filling vugs of late-stage quartz (q_2; *BSE*). **d** Oxide-stage carbonatisation of host limestone: coarsening of calcite grains (*cc*) and precipitation of Mn–Fe oxyhydroxides (*ox*) in open spaces. Note the newly formed authigenic quartz (*q*; *BSE*). **e** Rhythmic precipitation of Pb–APS minerals and Pb arsenates in pore spaces between second-stage quartz crystals (q_2; BSE image). **f** Intergrown Pb arsenates and Zn arsenates filling vugs between late-stage quartz crystals (q_2). **g** Field photograph of mansfieldite "sinter" layer formed on leached limestone. **h** Back-scattered image showing paragenetic association of mansfieldite (*msf*) with oxide-stage pyrite (*py*) and euhedral, authigenic quartz (*q*). *BSE* back-scattered electron image

primary gold was bound up in arsenian pyrite. Dissolution of such pyrite during the oxide stage could have liberated gold, which was then re-deposited in the oxide ore zone.

Although a number of whole-rock samples have anomalous gold and silver contents, gold and silver were generally invisible in polished section, and gold could not be detected by conventional EMP techniques. Preliminary trace element analysis of pyrite using an electron probe microanalyser yielded Au concentrations of 40–50 ppm (Johanson, personal communication). The highest whole-rock gold grade (45 ppm) occurs in cinnabar-rich jasperoidal rocks ("silica mud"). The gold, which is of high purity, occurs within or close to pore spaces and was precipitated last (Fig. 10a). The Au-rich sample also contains 30 ppm Ag, which is probably encapsulated in cinnabar (Table 5) because gold grains contain no Ag. Gold grains in this sample exhibit spongy, pitted surfaces.

Native gold also occurs within the Fe–Mn oxyhydroxide ore, and in massive goethite–barite (3.8 ppm) and scorodite

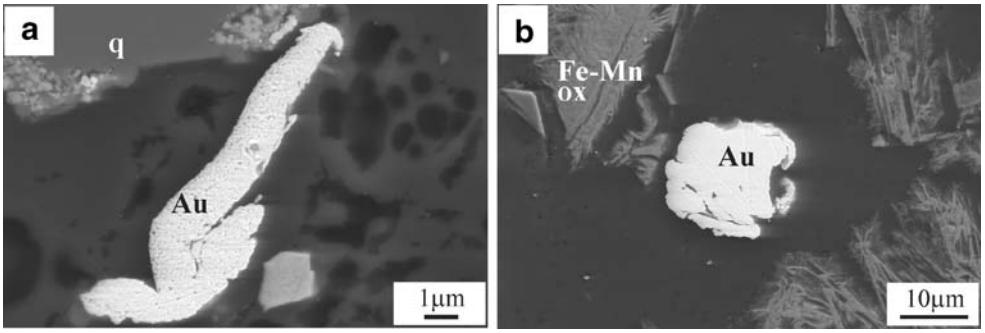

Fig. 10 Back-scattered electron images of native gold. **a** Gold grain with pitted surface in a vug of cinnabar-rich "silica mud" (*q*). **b** Supergene gold associated with late, needle-like Fe–Mn oxides

rocks (5.9 ppm). It seems to have been precipitated very late in pore spaces of the oxide ore stage (Fig. 10b). These gold grains have smooth surfaces, as opposed to those of the sulphide ore stage. There is a correlation between high Ag grades (up to 96 ppm) and abundance of Pb sulphide, Pb sulphosalts and complex Pb oxides in the oxide ore samples, which suggests that Ag is bound with Pb minerals.

Discussion

Comparison with Carlin-type ores

Although similar in many aspects to Carlin-type precious metal deposits, the sedimentary rock-hosted disseminated gold deposits of the Takab region differ in some respects, most notably in their close spatial and temporal relationship with volcanic–hydrothermal activity and the mechanism of ore precipitation (Alvarez and Noble 1988; Bakken et al. 1989; Berger and Bonham 1990; Kuehn and Rose 1995; Turner et al. 1994; Arehart 1996; Ilchik and Barton 1997; Weaver and Cline 1999; Hofstra et al. 1999; Hofstra and Cline 2000; Cline and Hofstra 2000; Cline 2001; Cail and Clain 2001; Emsbo et al. 2003; Ressel and Henry 2006).

Diagnostic features of the disseminated gold deposits of the Takab region compared to Carlin deposits include:

1. Age of mineralisation—Cenozoic.
2. Lithology—Intercalated carbonaceous pelite and carbonate rocks (Zarshouran) or purely carbonate rocks (Agdarreh); formation of local free carbon.
3. Structural and lithological controls—Deep crustal faults, proximal thrust faults, normal faults, strike–slip duplexes and extensional structures.
4. Alteration—Multi-phase decalcification and silicification. Argillic alteration is minor.
5. Metal anomalies—At Carlin-type deposits in the USA, the sulphide stage shows enrichment in Au, Ag, As, Sb, Tl, Hg, ±Te, ±Se and ±W with high Au/Ag ratios (20–30), and low to nil contents of base metals. Compared to Calin-type deposits, the Takab ores contain Zn and Pb minerals and have typically high Zn/Pb ratios.
6. Mineralogy—Abundant quartz, pyrite, arsenian pyrite, realgar, orpiment, cinnabar and traces of getchellite, tellurian minerals, invisible gold and barite. Sphalerite, galena and less abundant Pb sulphosalts occur in the Takab ores, and fluorite is present at Zarshouran.
7. Depth of formation—In Carlin-type ores, depths vary from shallow epizonal to 2–5 km (Kuehn and Rose 1995; Hofstra and Cline 2000). The Agdarreh mineralisation, however, seems to have formed at shallower depths.

Depositional milieu

Epithermal systems and modern geothermal activity in the region of Takab have a close spatial and temporal relationship with Late Cenozoic to Quaternary, shallow-level magmatic activity. They form part of a hydrothermal Cu–Au and base metal province that extends along the Urumieh–Dokhtar volcanic belt from northwestern to southeastern Iran (Daliran et al. 2005). The gold deposits of northern Takab area show textures and mineral assemblages characteristic of geothermal settings as defined by Hedenquist et al. (2000). The northern Takab gold deposits occur in basement rocks and the Cenozoic sedimentary cover, in a location distal to known volcanic vents, and only differ from low-sulphidation epithermal deposits in being hosted by carbonate sedimentary rocks. Hydrothermal activity was common in the region, as indicated by the presence of extensive areas of altered Miocene volcanic rocks (kaolinite–alunite, GSI 1999b) 2 km east of the Agdarreh deposit and high-sulphidation style gold and copper mineralisation associated with alunite alteration (Daliran, unpublished data) as at the Touzlar deposit (see Fig. 2).

In the Takab region, voluminous arc magmatism formed in the Miocene in response to northeastward subduction of the Neo-Tethyan seafloor and the formation of syn-extensional basins west of the Geynardjeh thrust fault (GSI 1999b; Stockli et al. 2004). Topographic sagging, faulting and crustal thinning associated with subduction

enabled magmas to ascend to shallow levels and created a high geothermal gradient. Upflow of hydrothermal fluids associated with the Miocene volcanic activities in the Takab tectonic basin gave rise to epithermal deposits. Numerous fault-controlled, H_2S-bearing springs and solfatara are still active in association with large-scale travertine deposits that locally contain very high concentrations of gold, silver and other metals of the epithermal suite (Daliran 2003).

Several lines of evidence suggest that ore precipitation at Agdarreh was rapid and took place at low pressures and temperatures. The very fine-grained nature of the ore minerals, the quartz textures, and the presence of invisible gold, cinnabar, orpiment, realgar and getchellite are consistent with an epithermal environment (Seward 1984; Renders and Seward 1989; Dong et al. 1995; Cooke et al. 1996). The occurrence of travertine precipitates on the flanks of the Agdarreh and Zarshouran deposits suggests that the geothermal fluids reached the surface, although the maximum age of travertine formation is unknown. The extensive acid alteration and blanket-like geometry of the altered zones at Agdarreh show some similarities with hot spring precious metal deposits (Wells and Ghiorso 1988; Peters 1991; Hollister et al. 1992; Zimmerman and Larson 1994; Saunders and Schoenly 1995; Sherlock and Lehrman 1995; Ebert and Rye 1997). The local occurrence of siliceous rocks having a cryptocrystalline matrix and containing contorted cinnabar seams suggests that some surficial hydrothermal discharge took place, perhaps in a mud pool. Preliminary fluid inclusion data for hydrothermal quartz and barite show homogenisation temperatures of <200°C and fluid pressures of <500 bars. These fluid pressures correspond to shallow depths of ≤500 m; phase separation suggests that boiling occurred at this shallow depth (Daliran and Walther 2000; Daliran et al. 2002).

Paleogeographic reconstruction suggests that the top of the host reefal limestone was probably in a terrestrial environment and exposed during the deposition of the Upper Red Formation. The presence of erosional channels on the surface of the mineralised limestone, but a lack of mineralised clasts in the channel fillings, suggests that mineralisation post-dated the erosional phase. If any Upper Red Formation sediments were initially deposited on the reefal limestones, they have been subsequently removed by erosion. In this latter case, it is conceivable that the mineralisation could have formed up to a few hundred metres below the surface (the thickness of the Upper Red Formation). However, the host limestones have been affected by only minor uplift and tilting due to their location in the subsiding Takab basin and, therefore, erosion of any overlying sediments would have been limited.

The absolute age of mineralisation at Agdarreh cannot be determined because of the lack of appropriate minerals for dating. Geochronologic data from areas near the Zarshouran gold deposit indicate that volcanic activity occurred at 16.2 and 11.1 Ma, and mineralisation at 14.7±0.4 Ma (Mehrabi et al. 1999). At the hydrothermal Zn deposit of Angouran (mixed sulphide–nonsulphide ore) east of the Geynardjeh thrust, the volcanism that is most closely related with mineralisation has an age of 18.42±0.18 Ma (Daliran et al., unpublished). At Agdarreh, the lower limit of the mineralisation is defined by the Aquitanian–Burdigalian age of the host limestone (23.0 to 20.4 Ma; International Stratigraphic Chart 2005, http://www.stratigraphy.org). Although mineralisation is absent from the overlying Upper Red Formation (Miocene), it cannot be ruled out that it post-dated this formation, but formed within the underlying carbonate unit because of lithological controls on metal deposition.

Source of ore fluids

In typical epithermal precious metal systems, gold, silver, arsenic and antimony are thought to be transported mainly as bisulphide–sulphide complexes, but also as seleno- and tellurocomplexes (Seward 1984; Renders and Seward 1989; Shenberger and Barnes 1989; Benning and Seward 1996). Pyrite is the main host of gold in Carlin-type ores. Different fluid sources and depositional mechanisms have been proposed for pyrite precipitation in these deposits (Sillitoe and Bonham 1990; Kuehn and Rose 1995; Arehart et al. 1993; Arehart 1996; Ilchik and Barton 1997; Cline and Hofstra 2000; Rui-Zhong et al. 2002). One suggested mechanism for pyrite–gold precipitation involves sulphidation of ferroan minerals in the host rocks using H_2S derived mainly from sedimentary rocks (e.g. Cline and Hofstra 2000; Embso et al. 2003), although this mechanism alone might not account for the deposition of gold in Carlin-type deposits (Kesler et al. 2003).

Iron was clearly introduced by hydrothermal fluids, as the reefal limestones at Agdarreh initially contained no Fe-bearing minerals. The presence of active solfataras in the region of Takab suggests that the hydrothermal fluids were also capable of providing H_2S. Precipitation of metals in hydrothermal systems commonly results from the loss of H_2S vapor upon boiling and pressure reduction at or near the surface (Hedenquist and Henley 1985). Removal of the bisulphide ligands can then induce gold precipitation on a favourable substrate such as arsenian pyrite. At Agdarreh, rapid cooling of ascending fluids close to the surface would have changed the fluid properties and precipitated complexed metals such as gold. These processes were accompanied by silicification and decalcification of the host limestone. The huge losses of CO_2 may have promoted the precipitation of metals such as Au, Ag, As and Sb by destabilising the bisulphide–sulphide complexes (Henley 1984). High contents of elements such as Se, Te and Tl have been used to infer a magmatic input to the fluids in epithermal systems (Cocker 1993; Kelley et al. 1998; Cooke

Pre Ore-Stage/ Ore-Stage I	Ore-stage II	Late/Post Ore-Stage	Oxide Stage
			Supergene (geothermal steam-heated?)
Hypogene acid leaching (decalcification)			**Oxidation of sulfides, acid-leaching** **Decalcification, karsting**
Silicification quartz I ***(jasperoid)***	**Silicification quartz II** ***(vug/vein filling)***		Hg-sulfides±(Cl,Br), barite Oxyhydroxide **Mn-Fe** ± path-finder metals **Arsenate, sulfate**, phosphate, APS-minerals, carbonate Mn-As pyrite Native Au
early pyrite (high As) **pyrite I** **sphalerite I** (submicron Au?)	**Pyrite II (low-As)** **Sphalerite II**, Pb-sulfide Pb-Sb-sulfosalts, Pb-telluride (altaite) stibnite, getchellite, native Bi, F-apatite (submicron Au?)	**Open-space/vein** As-sulfides Hg-sulfides Native Au **late Sr-barite**	**Open space minerals carbonates**
Kaolinitisation (±illite) **Carbonatisation (calcite, dolomite)**			F-apatite(±REE), rutile detrital zircon

Fig. 11 Generalised mineral paragenesis at the Agdarreh gold deposit (common alteration types and minerals are in bold)

and Simmons 2000; Cooke and McPhail 2001; Pals et al. 2001). At Agdarreh and Zarshouran (Mehrabi et al. 1999; Asadi et al. 2000), anomalous contents of these metals suggest that the hydrothermal fluids contained a magmatic component. In the northern Takab area, precipitates forming at an active thermal spring contain up to 14 wt% Se (Daliran 2003). The presence of a magmatic component in the Agdarreh fluids is partly supported by stable isotope data (Daliran et al. 2002). In the late oxide stage of mineralisation, the occurrence of rare mercury sulphides containing Cl and Br ("corderoite"), in association with Cl-bearing oxide complexes, suggests that the ore fluids mixed with meteoric ground water containing halogens derived from evaporitic rocks of the Qom Formation.

Evolution of fluids

The reefal limestones at Agdarreh were infiltrated by relatively acid geothermal fluids, especially in proximity to the fault zones. These fluids leached carbonate from the country rocks and produced an increase in their porosity (pre-ore stage). Near the surface, boiling resulted in fluid expansion and decrease in pressure and temperature (Daliran and Walther 2000). This led to loss of H_2S and CO_2, changes in fluid pH and Eh and destabilisation of bisulphide–sulphide complexes. Surging, venting of near-surface hydrothermal fluids and eventual collapse of the geothermal system resulted in multiphase quartz precipitation, brecciation and precipitation of disseminated ore minerals in different stages (Fig. 11). The first phase of silicification produced fine-grained jasperoid, minor amounts of Mn-bearing calcite, traces of arsenian pyrite (py_{1a}) and a new (main) pyrite generation (py_{1b}) associated with sphalerite. The second silicification stage formed coarse quartz crystals (q_2) in microveins and vugs, renewed precipitation of pyrite and sphalerite and formation of Pb–Sb–As–sulphides–sulphosalts, Pb–telluride and native bismuth. Traces of phosphate minerals (F–apatite) were also precipitated during the second stage. During these processes, some gold was probably encapsulated in the sulphide minerals. The common lack of Cu minerals indicates that hydrothermal fluids were Cu-poor, as in many low-sulphidation deposits. Phosphorus was probably derived from the dissolution of the biogenic reefal host limestone. Late ore fluids were enriched in As and Hg and precipitated orpiment and cinnabar in open spaces. Locally, further precipitation of native gold in cinnabar-rich mud occurred. Some late ore fluids precipitated barite in veins; during this phase of hydrofracturing and fluid surging, the fluids were more oxidised.

Dissolved carbonate from the limestone and hydrothermal dolomite reprecipitated in porous limestones peripheral to the silicified and mineralised zones. Trace amounts of native bismuth, cinnabar, LREE-F–apatite and phosphate complexes and Sr-bearing phosphates were precipitated together with these carbonates.

Supergene oxidation and possible relationship with geothermal activity

Oxidation processes have improved the recoverability of refractory gold that was initially contained in sulphides.

Oxidation probably occurred partly during the waning stages of hydrothermal activity and partly during recent geothermal activity; the latter process could have oxidised sulphides and remobilised Au into open spaces (cf. Hedenquist et al. 1994). At Agdarreh, co-precipitation of cinnabar and barite with oxide-stage Mn–Fe-rich minerals suggests that geothermal activity continued into the oxide stage. Colloidal aggregates of Mn-bearing pyrite may represent a transition to the oxidised fluids. In addition, abundant travertine in the Agdarreh area documents geothermal activity that could have been coeval with oxide-stage reactions. Mercury enrichment (cinnabar at Agdarreh) characterises the near-surface environment (Hedenquist and Arribas 1999).

The porous, karstified, sub-horizontal host limestones provided aquifers for oxidised ground water. Oxide minerals were precipitated within jasperoid blankets or replaced the leached limestone. Oxidative acid alteration and leaching led to enrichment in As and residual Al, and resulted in the formation of extensive Mn–Fe-rich oxyhydroxides, goethite, arsenates, gibbsite–bayerite and metre-scale outcrops of mansfieldite and trace amounts of APS minerals, phosphates (REE), Ca–Mn±Mg carbonates, kaolinite and Ca-sulphate. The oxide-stage processes were accompanied by widespread precipitation of minor amounts of "authigenic" quartz. Similar phosphate, sulphate and arsenate minerals occur in Carlin-type deposits in the USA (Arehart et al. 1992; Hostra and Cline 2000). These minerals, which precipitate under relatively acid conditions, can be either supergene or hypogene (Stoffregen and Alpers 1987; Muntean et al. 1990; Ashley et al. 1997; Dutrizac and Jambor 2000). At Agdarreh, chlorine in complex oxyhydroxides may have been derived from saline ground waters that circulated through the evaporatic rocks of the Cenozoic Qom Formation. By contrast, phosphorus was probably leached from the biogenic reefal limestones. The presence of Mn oxyhydroxides and the local occurrence of gold-bearing mud-like silica and cinnabar precipitates suggest that some mineralisation occurred in a surface environment, similar to hot spring-type gold ores (Panteleyev 1996). Mn was likely introduced into the system by late geothermal activity, given the low Mn content of the host limestones and the lack of Mn in the precursor sulphides. Mn-oxide mineralisation forms small deposits in the northwestern part of the Takab region (e.g. Dabal Kuh).

Conclusions

Miocene to Quaternary high-level magmatism in the Cenozoic extensional graben of Takab initiated a long history of hydrothermal activity that formed gold mineralisation in different host rocks, including the Cenozoic reefal limestone at Agdarreh. H_2S-bearing hot springs are still active and are precipitating various metals, including gold and silver. Large areas of travertine are also being formed.

Hydrothermal fluids have altered and leached large areas of the reefal limestone at Agdarreh, and produced largely bedding-controlled silicification and mineralisation of the host limestone. Jasperoids contain invisible gold and a suite of metals commonly associated with epithermal ore deposits. Early fluids produced silicification and precipitation of (auriferous) arsenian pyrite and sphalerite. Late fluids filled open spaces with As-sulphides, cinnabar and barite; high amounts of native gold were locally deposited with cinnabar. Oxidation of sulphide minerals and re-precipitation of metals resulted in the formation of a surficial blanket of complex Mn–Fe-rich oxyhydroxides and arsenate–phosphates (±sulphates). This process also released gold from refractory sulphides and increased gold contents to economic values of native gold. Oxidation processes may have been promoted by subsequent and ongoing geothermal activity.

The Agdarreh deposit shows numerous similarities with the Carlin gold deposits of Nevada. The combined field, petrographic and geochemical evidence indicates that Agdarreh formed as part of an epithermal gold system related to Cenozoic arc volcanism and shallow geothermal activity within the topographically low region of the Takab graben.

Acknowledgements Financial support for this research was provided by the German Research Foundation (DFG). I would like to thank M. Momenzadeh for drawing my attention to the northern Takab gold field, and A. Houshmand Zadeh and M. Ghorbani for sharing their geological knowledge of this area. The Ministry of Mines and Metals of Iran and Zarcan International kindly provided logistical support in Iran. The following persons are acknowledged for their analytical assistance: V. Zibat (EMP, University of Karlsruhe), W. Smykatz-Kloss and G. Istrate (XRD, University of Karlsruhe), B. Johanson (Geological Survey of Finland; trace gold), and M. Tarkian (University of Hamburg; sulphosalts). I would particularly like to thank J. Walther (University of Karlsruhe) for his discussions and encouragement throughout this project. A. Hofstra (USGS) is thanked for his constructive discussions of Carlin-type deposits. Critical comments and suggestions by Mineralium Deposita reviewers J. Cline, an anonymous reviewer, and I. Plimer were very useful in improving an earlier version of the manuscript. T.J. Barrett is thanked for improving the English and making helpful editorial suggestions.

References

Alavi M (1994) Tectonics of the Zagros orogenic belt of Iran; new data and interpretations. Tectonophysics 229:211–238

Alavi M, Hajian J, Amidi M, Bolourchi H (1982) Geology of the Takab-Saein-Qal'eh. Geol Surv Iran, Rpt 50, 99p

Alvarez AA, Noble DC (1988) Sedimentary rock-hosted disseminated precious metal mineralization at Pusisima Concepcion, Yauricocha district, central Peru. Econ Geol 83:1368–1378

Arehart GB (1996) Characteristics and origin of sediment-hosted disseminated gold deposits: a review. Ore Geol Rev 11:383–403

Arehart GB, Kesler SE, O'Neil JR, Foland KA (1992) Evidence for the supergene origin of alunite in sediment-hosted micron gold deposits, Nevada. Econ Geol 87:263–270

Arehart GB, Chryssoulis SL, Kesler S (1993) Gold and arsenic in iron sulfides from sediment-hosted disseminated gold deposits: Implications for depositional processes. Econ Geol 88:171–185

Asadi HH, Voncken JHL, Kühnel RA, Hale M (2000) Petrography, mineralogy and geochemistry of the Zarshouran Carlin-like gold deposit, northwest Iran. Miner Depos 35:656–671

Ashley PM, Lottermoser BG, Scott KM (1997) Supergene iron phosphate minerals in Proterozoic ironstones from the Olary Block, South Australia. N Jb Miner Mh 7:309–327

Bakken BM, Hochella MF, Marshall AF, Turner AM (1989) High resolution microscopy of gold in unoxidised ore from Carlin mine, Nevada. Econ Geol 84:171–179

Benning LG, Seward TM (1996) Hydrosulfide complexing of Au (I) in hydrothermal solutions 150–400°C and 500–1500 bar. Geochim Cosmochim Acta 11:1849–1871

Berger BR, Bonham HF (1990) Epithermal Au–Ag deposits in the western United States. J Geochem Explor 36:103–142

Cail LT, Clain JS (2001) Alteration associated with gold deposition at the Getchell Carlin-type gold deposit, north-central Nevada. Econ Geol 96:1343–1359

Cline JS (2001) Timing of gold and arsenic sulfide mineral deposition at the Getchell Carlin-type gold deposit, north-central Nevada. Econ Geol 96:75–89

Cline JS, Hofstra AH (2000) Ore-fluid evolution at the Getchell Carlin-type gold deposit, Nevada, USA. Eur J Mineral 12:195–212

Cocker MD (1993) Primary element dispersal in a carbonate-hosted, epithermal, high-grade, Au–Ag telluride system: Mayflower mine, Madison County, Montana, USA. J Geochem Explor 47:377–390

Cook NJ, Chryssoulis SL (1990) Concentrations of "invisible gold" in the common sulfides. Can Miner 28:1–16

Cooke DR, Simmons SF (2000) Characteristics and genesis of epithermal gold deposits. Rev Econ Geol 13:221–244

Cooke DR, McPhail DC (2001) Epithermal Au–Ag–Te mineralization, Acupan, Baguio district, Philippines: numerical simulations of mineral deposition. Econ Geol 96:109–131

Cooke DR, McPhail DC, Bloom MS (1996) Epithermal gold mineralization, Acupan, Baguio district, Philippines: geology, mineralization, alteration, and thermochemical environment of ore deposition. Econ Geol 91:243–272

Daliran F (2003) Discovery of 1.2 kg/t gold and 1.9 kg/t silver in mud precipitates of a cold spring from the Takab geothermal field, NW Iran. In: Eliopoulos D et al (eds) Mineral exploration and sustainable development. Millpress, Rotterdam, pp 461–464

Daliran F, Walther J (2000) A comparative study of the sediment-hosted gold deposits of Agdarreh and Zarshouran at N-Takab geothermal field, NW-Iran. Part II: fluid inclusion study. Bh Eur J Miner 12:32

Daliran F, Hofstra AH, Walther J, Stüben D (2002) Agdarreh and Zarshouran SRHDG deposits, Takab region, NW-Iran. GSA Annual Meeting 2002, Abstr with Prog, Session 63-8

Daliran F, Paar W, Neubauer F, Rashidi B (2005) New discovery of epithermal gold at Chahnali prospect, Bazman volcano, SE-Iran. In: Mao J, Bierlein FP (eds) Mineral deposit research: meeting the global challenge. Springer, Berlin, pp 917–919

Dong G, Morrison GW, Jaireth S (1995) Quartz textures in epithermal veins, Queensland—classification, origin and implications. Econ Geol 90:1841–1856

Dutrizac JE, Jambor JL (2000) Jarosite and their application in hydrometallurgy. Rev Mineral Geochem 40:405–452

Ebert SW, Rye RO (1997) Secondary precious metal enrichment by steam-heated fluids in the Crofoot–Lewis hot spring gold–silver deposit and relation to paleoclimate. Econ Geol 92:578–600

Emsbo P, Hofstra AH, Lauha EA, Griffin GL, Hutchinson RW (2003) Origin of high-grade gold ore, source of ore fluid components, and genesis of the Meikle and neighboring Carlin-type deposits, Northern Carlin Trend, Nevada. Econ Geol 98: 1069–1105

GSI, Geological Survey of Iran (1999a) Geological map of Iran 1:100,000 series, Sheet 5363, Shahindezh

GSI, Geological Survey of Iran (1999b) Geological map of Iran 1:100,000 series, Sheet 5463, Takht-e-Soleyman

GSI, Geological Survey of Iran (2000) Geological map of Iran 1:100,000 series, sheet 5462, Takab

Ghorbani M (2000) Petrological study of Cenozoic–Quaternary magmatic rocks and metallogeny of Takab area. Ph.D. Thesis, Shahid Beheshti University, Tehran, 430 p

Hedenquist JW, Henley RW (1985) Hydrothermal eruptions in the Waiotapu geothermal system, New Zealand: their origin, associated breccias and relation to precious metal mineralization. Econ Geol 80:1640–1668

Hedenquist JW, Arribas A (1999) The tops and bottoms of high-sulfidation epithermal ore deposits. Proc 5th Bienn SGA Meet and 10th Quad IAGOD Symp, pp 515–518

Hedenquist J, Arribas AR, Gonzalez-Urien E (2000) Exploration for epithermal gold deposits. Rev Econ Geol 13:245–277

Hedenquist JW, Matsuhisa Y, Izawa E, White NC, Giggenbach WF, Aoki M (1994) Geochemistry, and origin of high sulfidation Cu–Au mineralization in the Nansatsu District, Japan. Econ Geol 89: 1–30

Henley RW (1984) Chemical structure of geothermal systems. Rev Econ Geol 1:9–28

Hofstra AH (2002) Diverse origins of sedimentary rock-hosted disseminated gold deposits worldwide: overview. GSA Annual Meeting 2002, Abstr with Prog, Session 63-1

Hofstra AH, Cline JS (2000) Characteristics and models for Carlin-type deposits. Rev Econ Geol 13:163–220

Hofstra AH, Snee LW, Rye RO, Folger HW, Phinisey JD, Loranger RL, Dahl AR, Naeser CW, Stein HJ, Lewchuk M (1999) Age constraints on Jerritt Canyon and other Carlin-type gold deposits in the western United States—relationship to mid-Cenozoic extension and magmatism. Econ Geol 94:769–802

Hollister V, Hruska D, Moore R (1992) A mine-exposed hot spring deposit and related epithermal gold resources. Econ Geol 87:421–424

Ilchik RP, Barton MD (1997) An amagmatic origin of Carlin-type gold deposits. Econ Geol 92:269–288

Karimi M (1993) Petrographic-mineralogical studies, and the genesis of the Au–As ore at Zarshouran (Takab). M.Sc. Thesis, University of Tarbiat Moallem, Tehran, 264 p

Kelley KD, Romberger SB, Beaty DW, Pontius JA, Snee LW, Stein HJ, Thompson TB (1998) Geochemical and geochronological constraints on the genesis of Au–Te deposits at Cripple Creek, Colorado. Econ Geol 93:981–1012

Kesler SE, Fortuna J, Ye Z, Alt JC, Core DP, Zohar P, Borhauer J Chryssoulis SL (2003) Evaluation of the role of sulfidation in deposition of gold, Screamer section of the Betze-Post Carlin-type deposit, Nevada. Econ Geol 98:1137–1157

Kuehn CA, Rose AW (1995) Carlin gold deposits, Nevada. Origin in a deep zone of mixing between normally pressured and overpressured fluids. Econ Geol 90:17–36

Mehrabi B, Yardley BWD, Cann JR (1999) Sediment-hosted disseminated gold mineralisation at Zarshuran, NW Iran. Miner Depos 34:673–696

Mineral Export Company (1995) Geological map of Agdarreh 1:5000 (intern doc)

Mineral Export Company (1996) Geological cross sections at Agdarreh 1:1,000, Sheets A–K (intern doc)

Muntean JL, Kesler SE, Russel N, Polanco J (1990) Evolution of the Monze Negro acid sulfate Au–Ag deposit, Pueblo Viejo,

Dominican Republic: important factors in grade development. Econ Geol 85:1738–1758

Pals DW, Spry PG, Chryssoulis C (2001) Unusually high submicroscopic gold and arsenic contents of pyrite from the Emperor gold deposit, Fiji. Proc 6th Bienn SGA-SEG Meeting, Krakow, Poland, pp 799–802

Panteleyev A (1996) Hot-spring Hg. In Lefebure DV and Hoy T (eds) Selected British Columbia mineral deposit profiles. Volume 2—metallic deposits. British Columbia Ministry of Employment and Investment, Open File 1996-13:31–32

Persian Resources (1995) Report on exploration at Agh Darreh, West Azarbaijan province, Islamic Republic of Iran, June 1994–December 1994 (intern rpt)

Peters EK (1991) Gold-bearing hot spring systems of the northern Coast Ranges California. Econ Geol 86:1519–1528

Renders PJ, Seward TM (1989) The adsorption of thio gold (I) complexes by amorphous As_2S_3 and Sb_2S_3 at 25 and 90°C. Geochim Cosmochim Acta 53:255–267

Ressel MW, Henry CD (2006) Igneous geology of the Carlin Trend, Nevada: development of the Eocene Plutonic complex and significance for Carlin-type gold deposits. Econ Geol 101:347–383

Robinson BW, Graham J (1992) Advances in electron microprobe trace element analysis. J Comput-assist Microsc 4:263–265

Rui-Zhong H, Wen-Chao S, Xian-Wu B, Guang-Zhi T, Hofstra AH (2002) Geology and geochemistry of Carlin-type gold deposits in China. Miner Depos 37:378–392

Saunders JA, Schoenly PA (1995) Boiling, colloidal nucleation and aggregation, and the genesis of bonanza Au–Ag ores of the Sleeper deposit, Nevada. Miner Depos 30:199–210

Seward TM (1984) The transport and deposition of gold in hydrothermal systems. In: Foster RP (ed) Gold metallogeny and exploration. Chapman and Hall, London, pp 165–181

Shenberger DM, Barnes HL (1989) Solubility of gold in aqueous sulfide solutions from 150 to 350°C. Geochim Cosmochim Acta 53:269–278

Sherlock RL, Lehrman NJ (1995) Occurrences of dendritic gold at the McLaughlin mine hot-spring gold deposit. Miner Depos 30:323–327

Simon G, Kesler SE, Chyssoulis S (1999) Geochemisty and textures of gold-bearing arsenian pyrite, Twin Creek, Nevada: implication for deposition of gold in Carlin-type deposits. Econ Geol 94:405–422

Sillitoe RH, Bonham HF (1990) Sediment-hosted gold deposits: distal products of magmatic–hydrothermal systems. Geology 18:157–161

Stockli D, Hassanzadeh J, Stockli L, Axen G, Walöker JD, Terrence TJ (2004) Structural and geochronological evidence for Oligo-Miocene intra-arc low-angle detachment faulting in the Takab–Zanjan area, NW Iran. Geol Soc Amer Abstr Progr 36(5):319

Stöcklin J (1968) Structural history and tectonics of Iran: a review. Am Assoc Pet Geol Bull 52:1229–1258

Stoffregen RE, Alpers ChN (1987) Woodhouseite and svanbergite in hydrothermal ore deposits: products of apatite destruction during advanced argillic alteration. Can Miner 25:201–211

Turner SJ, Flindell PA, Hendri DH, Hardjana I, Lauricella PF, Lindsay RP, Marpaung B, White GP (1994) Sediment-hosted gold mineralization in the Ratatotok district, North Sulawesi, Indonesia. J Geochem Explor 50:317–336

Weaver KD, Cline JS (1999) Geochemistry of ore-stage and non-ore pyrite and marcasite from the Getchell Carlin-type gold deposit, Nevada. Geol Soc Amer Abstr Progr 31:A10

Wells JT, Ghiorso MS (1988) Rock alteration, mercury transport, and metal deposition at Sulfur Bank, California. Econ Geol 83:606–618

Zimmerman BS, Larson PB (1994) Epithermal gold mineralization in a fossil hot spring system, Red Butte, Oregon. Econ Geol 89:1983–2002